Journal of Structural Geology, Vol. 13, No. 8, pp. 865 to 886, 1991
Printed in Great Britain

0191-8141/91 $03.00 + 0.00

Analysis of minor fractures associated with joints and faulted joints

KENNETH M. CRUIKSHANK, GUOZHU ZHAO and ARVID M. JOHNSON

M. King Hubbert Structural Geology Laboratory, Department of Earth and Atmospheric Sciences, Purdue University, West Lafayette, IN 47907, U.S.A.

(*Received* 6 *April* 1990; *accepted in revised form* 7 *April* 1991)

Abstract—In this paper, we use fracture mechanics to interpret conditions responsible for secondary cracks that adorn joints and faulted joints in the Entrada Sandstone in Arches National Park, U.S.A. Because the joints in most places accommodated shearing offsets of a few mm to perhaps 1 dm, and thus became faulted joints, some of the minor cracks are due to faulting. However, in a few places where the shearing was zero, one can examine minor cracks due solely to interaction of joint segments at the time they formed.

We recognize several types of minor cracks associated with subsequent faulting of the joints. One is the kink, a crack that occurs at the termination of a straight joint and whose trend is abruptly different from that of the joint. Kinks are common and should be studied because they contain a great deal of information about conditions during fracturing. The sense of kinking indicates the sense of shear during faulting: a kink that turns clockwise with respect to the direction of the main joint is a result of right-lateral shear, and a kink that turns counterclockwise is a result of left-lateral shear. Furthermore, the kink angle is related to the ratio of the shear stress responsible for the kinking to the normal stress responsible for the opening of the joint. The amount of opening of a joint at the time it faulted or even at the time the joint itself formed can be estimated by measuring the kink angle and the amount of strike-slip at some point along the faulted joint.

Other fractures that form near terminations of pre-existing joints in response to shearing along the joint are horsetail fractures. Similar short fractures can occur anywhere along the length of the joints. The primary value in recognizing these fractures is that they indicate the sense of faulting accommodated by the host fracture and the direction of maximun tension.

Even where there has been insignificant regional shearing in the Garden Area, the joints can have ornate terminations. Perhaps the simplest is a veer, where the end of one joint segment turns gradually toward a nearby joint segment. The veer is a result of a nearby, shear-stress-free face such as a joint surface. Our greatest difficulty has been explaining long overlap of parallel joint segments, that is, the lack of veer. The only plausible explanation we know is suggested by the research of Cottrell and Rice, that high compression parallel to the joint segments will tend to prevent the joints from turning toward one another.

The most interesting and puzzling fractures are stepped joints and associated echelon cracks, in which the slight misalignment of the stepped joints suggests mild left-lateral shear, while the strong misalignment of echelon cracks that continue the traces of the stepped joints suggests strong right-lateral shear. The stepped joints are thought to reflect local left-lateral shearing that acted over an area of several thousand square metres, whereas the stepped echelon cracks reflect local interaction between the tips of nearby joints propagating in different directions.

INTRODUCTION

THE understanding of rock fracture has progressed far enough for us to infer conditions of faulting and jointing from the forms of faults and joints, provided their geologic history has been simple. Studies combining theoretical and field work have provided basic rules with which we can interpret conditions responsible for echelon cracks, tail cracks and bridge fractures associated with joints or faulted joints.

The purpose of this paper is to use the understanding of fracturing to develop some rules for interpreting traces of secondary cracks associated with joints and faulted joints. Our examples are along fractures in Entrada Sandstone in the Garden Area (Fig. 1) of Arches National Park, near Moab, Utah, although Segall & Pollard (1983a) and Davies & Pollard (1986) have described analogous secondary cracks on joints and faulted joints in Sierran granite.

The Garden Area provides an excellent opportunity to study joints and faulted joints. The area was subjected to two periods of jointing and two periods of strike-slip faulting—all were extremely mild deformations—so one can compare secondary cracks that formed where joints were subjected to negligible shearing with secondary cracks that formed where there was significant faulting following the jointing. Some of the secondary cracks appear to have formed at the same time as the joints themselves, a result of interaction between adjacent joint segments. Others appear to be individual kinks or groups of horsetail cracks that formed near terminations of pre-existing joints as a result of later faulting along the joints.

In most areas it is no simple matter to differentiate fractures that developed at the time the joints opened from fractures that developed when the joints subsequently slipped as faults. We are able to make such a differentiation in the Garden Area, however, because in part of the area there was only jointing (zero slip) and in other parts there was faulting following the jointing. The secondary fractures in the area of zero slip resulted from interaction of the joints at the time they formed, essentially in response to mode I loading, resulting from regional extension. In most parts of the Garden Area,

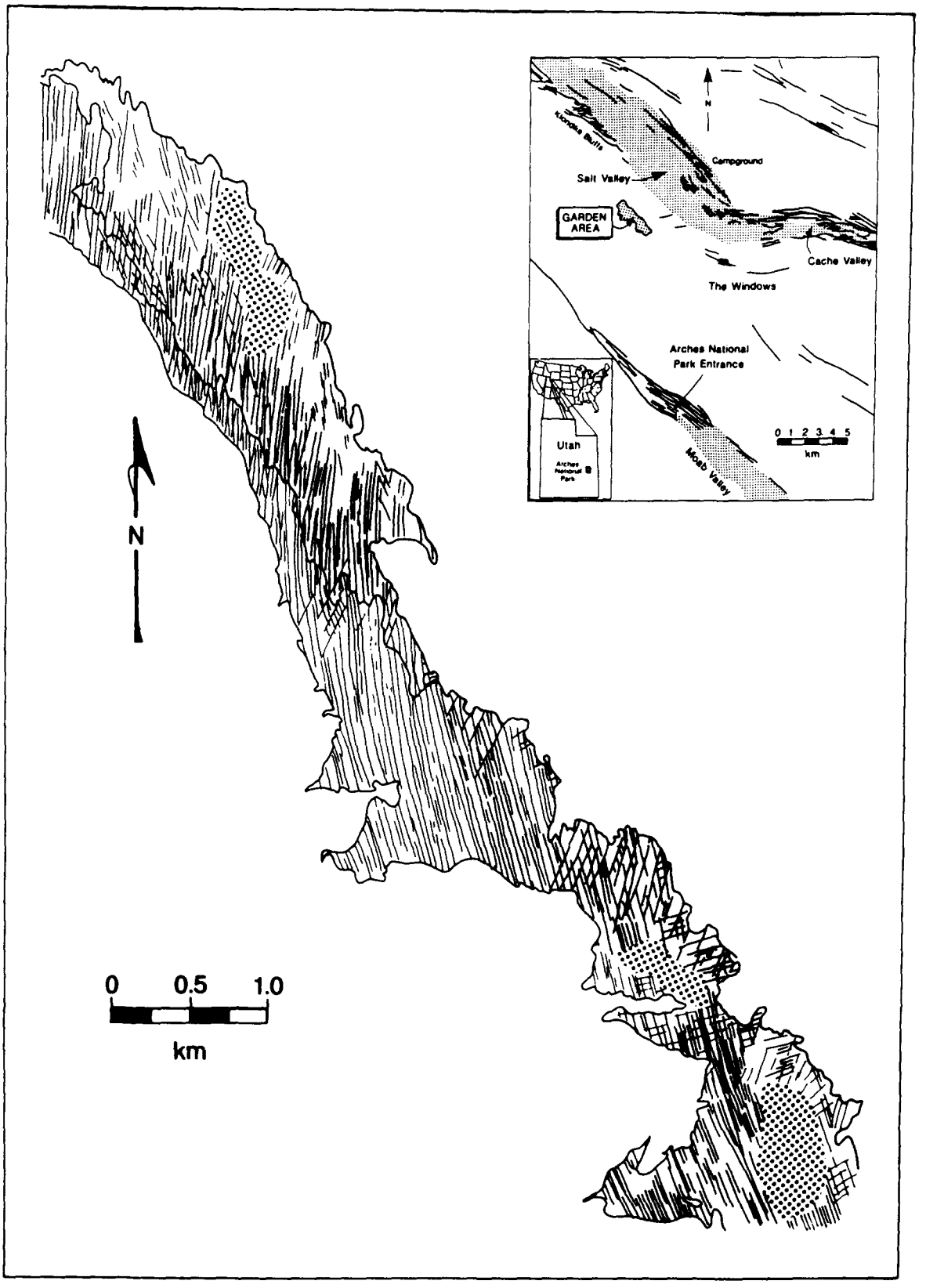

Fig. 1. The Garden Area of the Arches National Park, U.S.A., showing fracture traces visible on air photographs. Inset shows that the Garden Area is on the SW limb of the Salt Valley anticline.

the joints have subsequently been subjected to shearing (mode II and III deformations; Lawn & Wilshaw 1975): a left-lateral slip in the northern third and a right-lateral slip in the central half of the area (Fig. 2). Comparison of joint terminations between areas of shear and no shear allows us to examine secondary fractures that result from shearing superimposed on the joints, in addition to secondary fractures due to shear imposed through interaction.

The theoretical basis of our analyses is broad, but we rely most heavily on investigations of crack stability and effect of mode II shearing on mode I fracturing by

Cottrell & Rice (1980), Sumi *et al.* (1985) and Olson & Pollard (1989), and on the investigation of effects of mode III shearing on fracturing by Pollard *et al.* (1982). To study crack interactions, we use an alternating method similar to that explained by Pollard & Holzhausen (1979). Results of these analyses are applied to some field examples in order to infer conditions at the time the secondary cracks formed.

SETTING

The Garden Area is on the SW flank of the Salt Valley anticline, the northwesternmost of the salt-cored anticlines of the Paradox fold and fault belt in western Colorado and eastern Utah (Dane 1935, Elston *et al.* 1962, Cater & Craig 1970, Doelling 1985). The area is largely within Arches National Park, and about mid-distance between the Salt Valley anticline in the NE and the Moab fault zone in the SW (Fig. 1). The rocks in the Garden Area have been only mildly deformed and dip about 7° toward the SW.

The joints in the Garden area occur within the white sandstone of the Moab Member which, here, is about 10 m thick. According to Dyer (1988), underlying the Moab Member are 70–95 m of red, cross-bedded sandstone of the Slickrock Member, and overlying the Moab Member are about 12 m of thinly bedded, alternating claystone, sandstone and limestone, reinterpreted to be the lower part of the Morrison Formation (Cater & Craig 1970).

There are three sets of joints in the Garden Area (Fig. 2) which Dyer (1983) termed J-1, J-2 and J-3, with J-3 being the youngest. Traces of J-3 joints trend about N10°W throughout the Garden Area and dip vertically or steeply eastward. Joints J-1 trend about N60°E and occur only in the southern part of the area. Joints J-2 trend about N30°E and occur in both the northern and southern parts of the area (Fig. 2). Reinvestigation of the fractures (Zhao & Johnson in review) indicates that joints J-1 and J-2 are jointed faults; that is, they are band faults or fault zones that formed in a shearing (mode II or III) deformation and subsequently opened in mode I deformation, and are in this respect similar to stepped fault segments described in a large landslide in central Utah by Fleming & Johnson (1989). In the Garden Area, the trends of the J-1 and J-2 joints were inherited from the trends of strike-slip faults that formed in response to NE–SW compression. In the vicinity of joints J-2, joints J-3 degenerate into numerous short segments, bridge cracks or horsetail cracks, in some places oblique to the regional trend, particularly in the northern part of the area (Fig. 2), indicating that joints J-3 are younger than joints J-2, as indicated by Dyer (1983). Although Dyer decided that joints J-1 are the oldest, their age is unknown. Here we are going to discuss structures associated with the J-2 and J-3 joints of Dyer.

The J-3 joints are of the type Dyer (1983, 1988) called

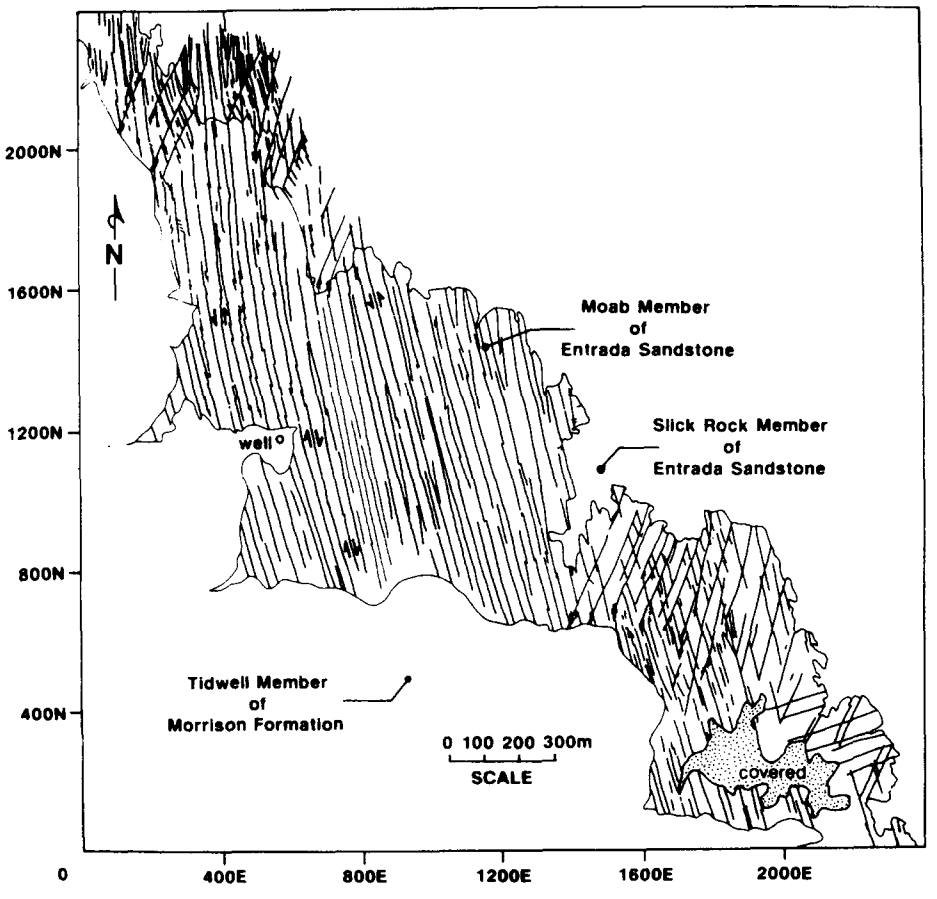

Fig. 2. Traces of systematic fractures—joints, faulted joints and jointed faults—in the Garden Area. There are three sets of joints in the area, trending about N10°W, N30°E and N60°E.

zoned, a type of systematic, composite joint in which individual joint segments tend to be parallel and confined to a narrow zone, but generally not coplanar with other individuals of the zone (Segall & Pollard 1983b). The zoned nature is characteristic of both plan and cross-section views of the joints (Dyer 1988). The zones of joints are confined to the Moab Member and degenerate into fringe fractures near the upper and lower contacts of this unit (Dyer 1983).

Figure 3(a) is a photograph taken toward the north from the well at co-ordinates 1200N, 500E (Fig. 2) and shows grooves that have been eroded along the zones of joints. Joints within one of the zones are shown in Fig. 3(b). Individual joints within a zone typically have traces a few meters to a few tens of meters long (Fig. 3b) and spacing between zones in the Garden Area generally is 20–45 m (Fig. 2), indicating that maximum dimensions of individual joints and the spacing between adjacent zones are of the order of the thickness of the Moab Member (Dyer 1983).

There are band faults (Aydin 1978) in most of the Garden Area striking N30°E or N60°E. They are older than the joints, so they provide convenient markers of lateral slip along the joints. According to Dyer (1983), the slip along the joints has been roughly horizontal, so the joints have become faulted joints and the faulting is strike-slip. The amount of slip along the faulted joints is different in different areas, but is generally a few mm to a few cm. Along one faulted joint in the eastern central part of the area, the slip is 9 cm.

Opposite senses of strike-slip along faulted joints in different parts of the Garden Area reflect inhomogeneous deformation within the region, but there are domains within which the sense of strike slip is the same (Fig. 2). In the northern third of the area, the sense of slip is consistently left-lateral. Within a narrow band trending NW–SE, about 300 m north of the well (co-ordinate 1600N 400E, Fig. 2), the amount of left-lateral slip reduces to zero and reverses to right-lateral slip. There are few data on slip in the southern part of the Garden Area, but the data we have suggest that the slip reverses, to become left-lateral again and farther south may reverse to become right-lateral. The picture that emerges is flexural slip of rock plates defined by vertical zoned joints, meaning that the axis of flexuring is vertical. This is the geologic setting of the joints and associated secondary fractures in the Garden area. The joints and faulted joints terminate in fractures with a wide variety of shapes, and the different shapes reflect different conditions at the time the joints formed, or at the subsequent time that the joints faulted. Here we investigate those conditions in terms of theoretical analyses of various combinations of mode I, II and III crack propagation.

KINKS

We begin with the simplest structures, the kinks. Figure 4(a) shows the trace of the end of a joint, occupying the lower half of the view, and a trace of a crack which juts forth about 0.15 m at an acute angle of about 43° into the country rock from the very tip of the joint. The crack is said to kink because its trend is abruptly different from that of the joint. The kink shown in Fig. 4(b) is similar to that shown in Fig. 4(a), but the kink angle is 50° and the kink is composed of three crack segments.

The setting of a kink similar to those shown in Fig. 4 is shown in the map in Fig. 5 of parts of several joint segments, long ones at the top and bottom, and three short segments in the middle. The joint at the bottom ends in the north in a kink whose trace is oriented 35° counter-clockwise with respect to the joint. The kink is about 0.1 m long and is sensibly straight.

Straight kinks

In order to develop criteria for differentiating secondary cracks that formed at the time the joints opened, when joint segments interacted, from secondary cracks that formed later, or when the joints slipped as faults, we follow theoretical analyses of shapes of mode I fractures by Cottrell & Rice (1980) and Sumi *et al.* (1985). The essential mechanical problem addressed in the two papers is: In the presence of far-field normal and shear stresses parallel and normal to a pre-existing crack, how will the crack begin to propagate and, approximately, what will be its path for small amounts of propagation?

A host of experimental, observational and theoretical evidence cited by Cottrell & Rice (1980) indicates that new crack growth in mode I on a pre-existing, straight crack will kink (i.e. suddenly change direction) if the straight crack is subjected to a combination of mode I and mode II loading, if the loading is sufficiently intense. They also show that the direction of kinking is the direction that maximizes the mode I stress-intensity factor and reduces to zero the mode II stress-intensity factor at the tip of the increment of new crack. The direction of kinking is, in principle, the same as the direction of crack propagation in a numerical, boundary-element model used by Olson & Pollard (1989) to investigate shapes of overlapping joints.

According to Cottrell & Rice (1980, equations 31), the mode I stress-intensity factor, K_I, at the tip of the increment of new crack, in terms of stress-intensity factors for the parent crack (k_I, k_{II}) (Fig. 6), is approximately

$$K_I = \tfrac{1}{4}[3\cos(\alpha/2) + \cos(3\alpha/2)]k_I - \tfrac{3}{4}[\sin(\alpha/2) + \sin(3\alpha/2)]k_{II} \quad (1a)$$

and the orientation of the increment of new crack is determined by solving the relation,

$$K_{II} = \tfrac{1}{4}[\sin(\alpha/2) + \sin(3\alpha/2)]k_I + \tfrac{1}{4}[\cos(\alpha/2) + 3\cos(3\alpha/2)]k_{II}.$$

For $K_{II} = 0$,

$$-\frac{k_{II}}{k_I} = \frac{\sin(\alpha/2) + \sin(3\alpha/2)}{\cos(\alpha/2) + 3\cos(3\alpha/2)} \quad (1b)$$

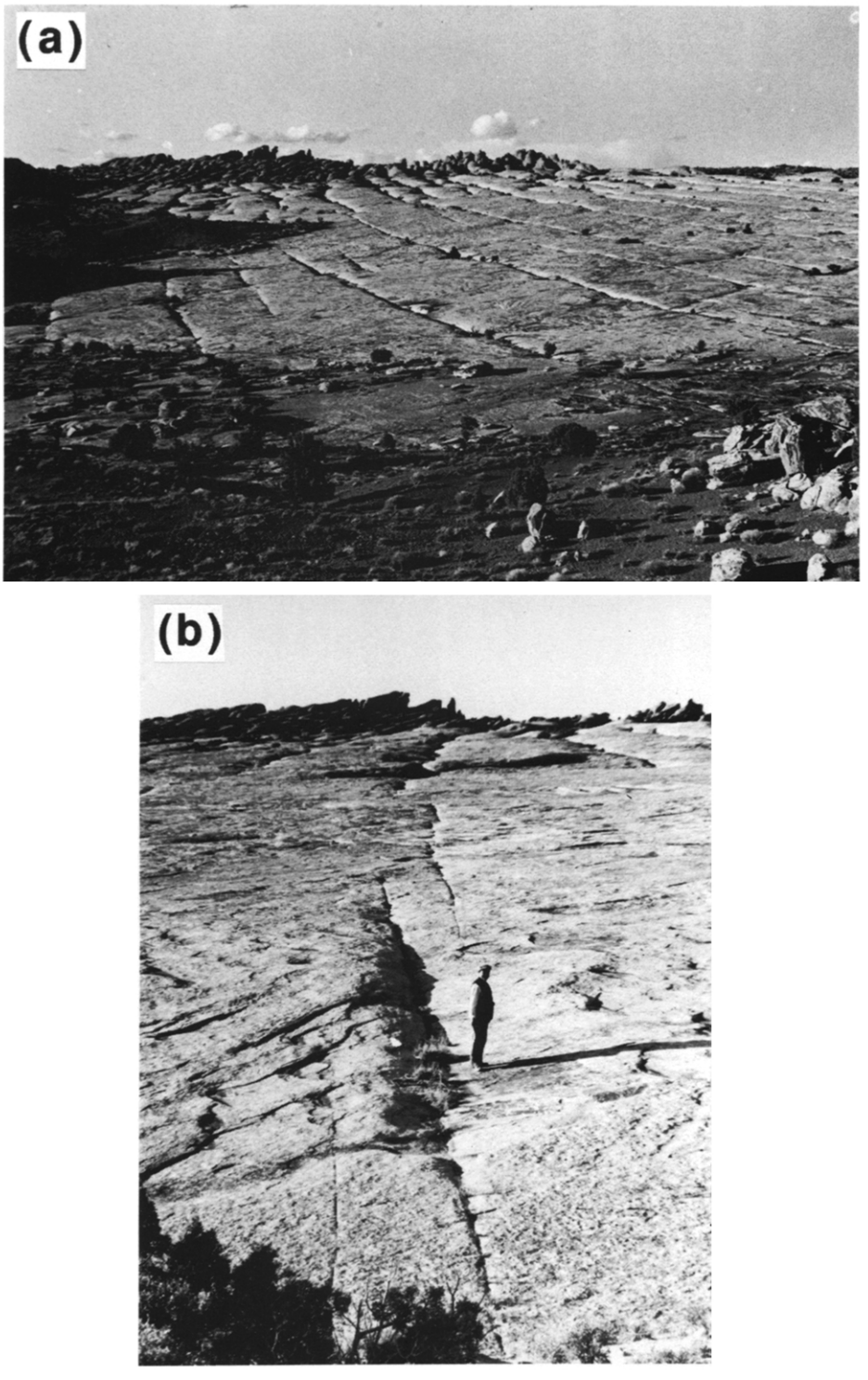

Fig. 3. Grooves eroded along joints in white Entrada Sandstone. View toward the north from near the well at the center of the Garden Area. (a) Zones of joints trend about N15°W in the foreground and N5°W in the distance. Spacing between zones of joints is generally 20–45 m. (b) Closer view of a zone of joints showing typical segments with traces a few meters to a few tens of meters long. (Guozhu Zhao for scale: 1.58 m.)

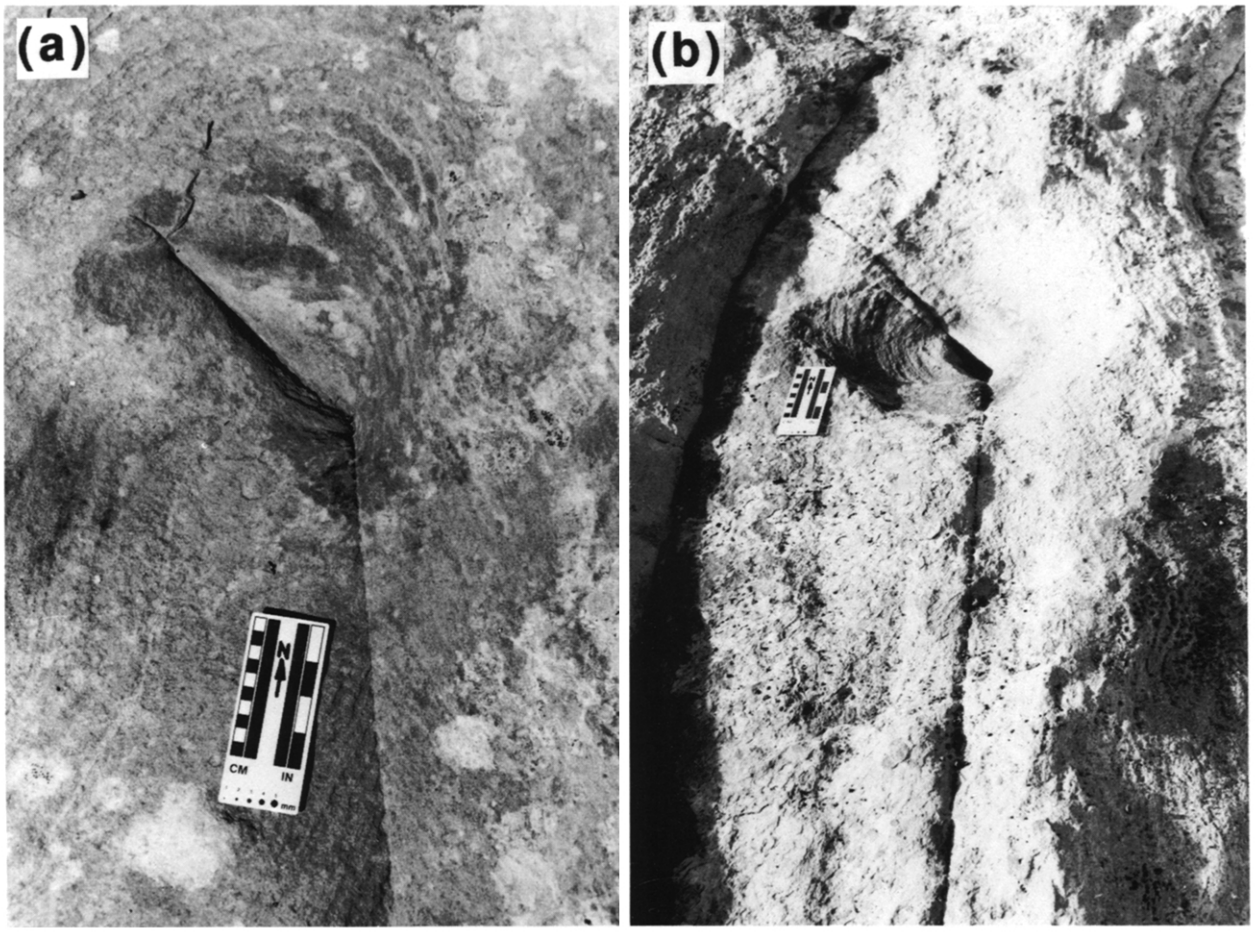

Fig. 4. Kinked ends of joints in northern part of the Garden Area. (a) Trace of joint enters lower part of view and ends in an abrupt kink fracture about 1.5 dm long that is oriented about 43° counter-clockwise with respect to the joint. Sense of shear responsible for kinking was left-lateral. (b) Similar kink fracture, but kink angle is about 50° and there are three crack segments in the area of the kink.

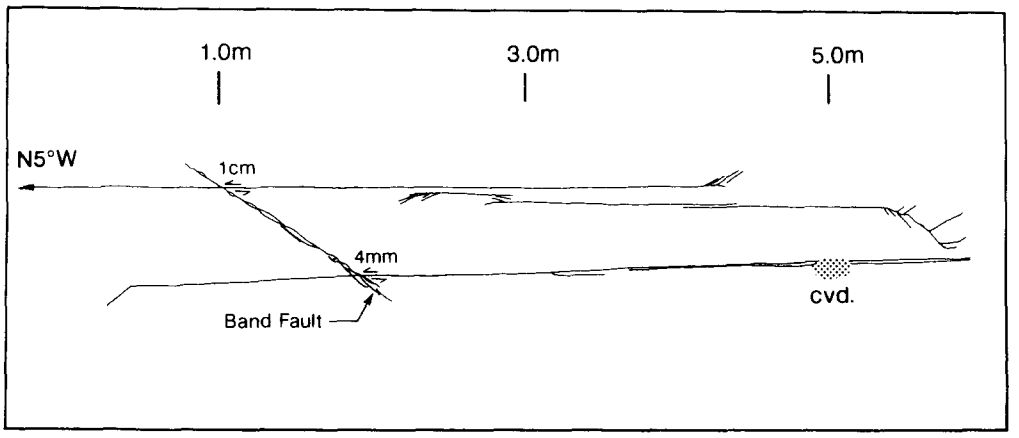

Fig. 5. Map of parts of several faulted joint segments and secondary fractures near their terminations in the northern part of the Garden Area, near co-ordinate 1800N 350E (Fig. 2). Amount of slip on faulted joints recorded in offset of band faults. The joint at the bottom ends in the north in a kink about 1 dm long that is oriented 35° counter-clockwise with respect to the trace of the joint.

for the counter-clockwise angle, α, between the x-axis and the direction of the increment of new crack. Here, for an isolated, straight crack subjected to uniform tractions and far-field stresses, the stress-intensity factors for the crack are:

$$k_I = (\sigma_{yy} + p)\sqrt{\pi a} \tag{2a}$$

$$k_{II} = \sigma_{xy}\sqrt{\pi a}. \tag{2b}$$

a is half crack length, p is fluid pressure in the crack, and σ_{yy} and σ_{xy} are far-field stresses; normal stresses are positive if tensile and pressure is positive if compressive.

Cottrell & Rice (1980) comment that equations (1a) and (1b) are within 5% agreement with exact results for kink angles as large as 40°. The solution to equation (1b) is given in Table 1 for positive values of k_{II}/k_I. For negative values, one merely multiplies all numbers in Table 1 by -1. The solution is also presented in Fig. 7(a), but in terms of ratios of far-field stresses rather than in terms of ratio of stress intensity.

Two extremes of equation (1b) are of particular interest. As the far-field shear stress becomes very large (k_{II}/k_I becomes large), the kink angle, defining the direction of incremental growth of the crack, is about 70.5° according to equation (1b); according to Cottrell & Rice (1980, fig. 6), the angle is about 76°. As the far-field shear stress becomes small (k_{II}/k_I becomes small), equations (1a) and (1b) become

$$K_I \approx (1 - \tfrac{3}{8}\alpha^2)k_I - \tfrac{3}{2}\alpha k_{II} \tag{3a}$$

$$\alpha \approx -2\frac{k_{II}}{k_I} = \frac{-2\sigma_{xy}}{\sigma_{yy} + p}. \tag{3b}$$

Combining equations (3a) and (3b),

$$K_I \approx k_I\left[1 + \tfrac{3}{2}\left(\frac{k_{II}}{k_I}\right)^2\right] = k_I[1 + \tfrac{3}{8}\alpha^2]. \tag{3c}$$

In all these results,

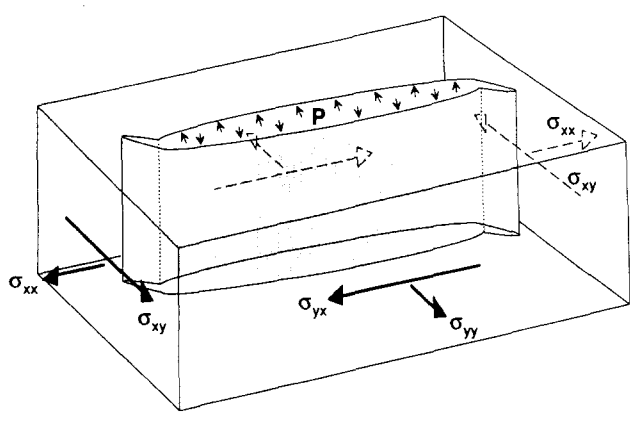

Fig. 6. Cartoon of kinked crack, showing positive stress state for a pressurized crack. Amount of opening is highly exaggerated.

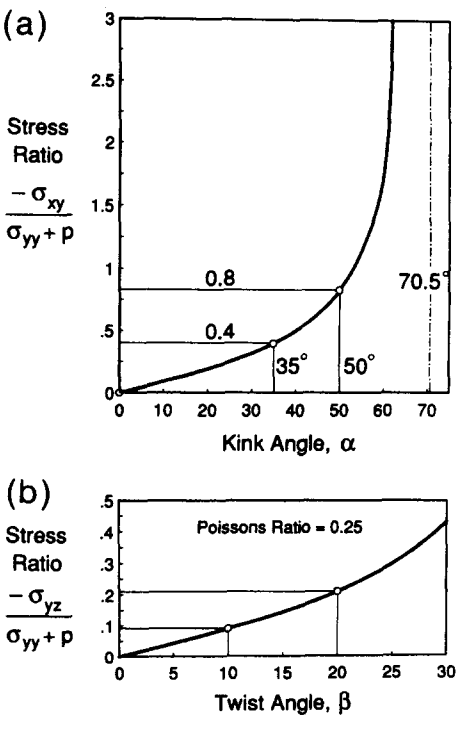

Fig. 7. Relations between ratio of far-field stresses and angle of kink or twist at end of a mode I fracture. (a) Kink angle, in degrees, is related to ratio of in-plane, mode II, shear stress σ_{xy} and mode I driving stress, $(\sigma_{yy} + p)$. (b) Twist angle is related to ratio of anti-plane, mode III, shear stress σ_{yz} and mode I driving stress.

Table 1. Relationship between kink angle, the stress-intensity factors at the tip of the parent fracture, and the amount of opening at the time the joint formed. These relationships are also shown in Figs. 7(a) and 10

Kink angle (α) (°)	Stress-intensity factor ratio (on parent crack) k_{II}/k_I	Joint opening/offset W_i/U
−1	0.0087	115
−2	0.0175	57
−3	0.0262	38
−4	0.0350	29
−5	0.0438	22.9
−6	0.0527	19.1
−7	0.0616	16.3
−8	0.0706	14.3
−9	0.0796	12.7
−10	0.0888	11.4
−15	0.1364	7.53
−20	0.1880	5.59
−25	0.2459	4.40
−30	0.3129	3.60
−35	0.3935	3.02
−40	0.4952	2.58
−45	0.6306	2.23
−50	0.8252	1.94
−55	1.1366	1.70
−60	1.7321	1.50
−65	3.3836	1.32
−70	36.06	1.17

Notes: Results for positive shear, shown in Fig. 8(a). For negative shear (Fig. 8b), multiply entries in this table by −1. $(k_{II}/k_I) = \sigma_{xy}/(\sigma_{yy} + p)$.

$$\left|\frac{k_{II}}{k_I}\right| \ll 1; \quad |\alpha| \ll 1. \tag{3d}$$

Thus the kink angle can be expressed simply (3b) for small values of mode II loading, and this simplification allows us to see more clearly how the Cottrell and Rice equations work. The results indicate that lengthening by pure mode I failure at the crack tip of a pre-existing crack will initiate with a kink and that the kink angle is a function of the stress state when lengthening initiates. The following results emerge.

(1) *Regardless of other elements of the stress state, if a straight crack begins to propagate when the loading is a combination of mode I (positive k_I, equation* 2a) *and mode II (positive or negative k_{II}, equation* 2b), *the resulting fracture will be kinked.* A reason that cracks kink if there is shear is shown in equation (3c); the mode I stress intensity factor for the extension, K_I, is larger if the fracture kinks ($\alpha \neq 0$) than it is if the fracture remains straight and propagates in its own plane ($\alpha = 0$).

(2) *The direction of the kink is determined by the sense of shear; thus if the far-field shear is right-lateral relative to the crack (positive), the kink angle is clockwise (negative)* (Fig. 8a); *and if the far-field shear is left-lateral relative to the crack (negative), the kink angle is counterclockwise (positive)* (Fig. 8b) *according to equation* (3b).

(3) *If the shear is large so that the magnitude of k_{II} is large compared to k_I, the magnitude of the kink angle may be as large as about* 75°, *and if the shear stress is nearly zero, the kink angle is nearly zero, equation* (3b).

Re-examining the fractures shown in Figs. 4(a) and 5, we would interpret the cracks at the ends to be simple kinks. For the kink shown in Fig. 4(a), the angle is

$$\alpha = +43°$$

so, according to Table 1, the stress ratio was about

$$\frac{\sigma_{xy}}{\sigma_{yy} + p} \approx -0.55 \qquad \text{(Result A)}$$

at the time the kink formed. We cannot specify the complete regional stress state because we have no information about σ_{xx} or, for that matter, σ_{yy} separately from pressure, p, in the crack.

For the kink shown in Fig. 5, the angle is

$$\alpha = +35°$$

so according to Table 1 and Fig. 7(a), the stress ratio was

$$\frac{\sigma_{xy}}{\sigma_{yy} + p} \approx -0.4. \qquad \text{(Result B)}$$

A third example is shown in Fig. 4(b), in which the kink consists of three short echelon cracks oriented at

$$\alpha \approx +50°.$$

The stress ratio for this kink was (Fig. 7a)

$$\frac{\sigma_{xy}}{\sigma_{yy} + p} \approx -0.8. \qquad \text{(Result C)}$$

In all three examples, the shear stress was left-lateral; all three examples are for faulted joints in the northern third of the Garden Area (Fig. 2).

Amount of opening of faulted joints

We can deduce more about the conditions responsible for kinking by examining the slip along the jointed faults. At the time a joint kinked, the width, W (Fig. 9),

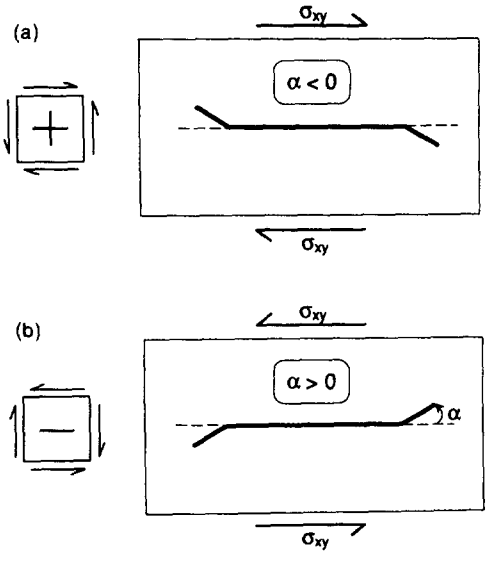

Fig. 8. Relations between sense of shear and direction of kinking. (a) For positive, right-lateral shear, the kink angle is negative. (b) For negative, left-lateral shear the kink angle is positive.

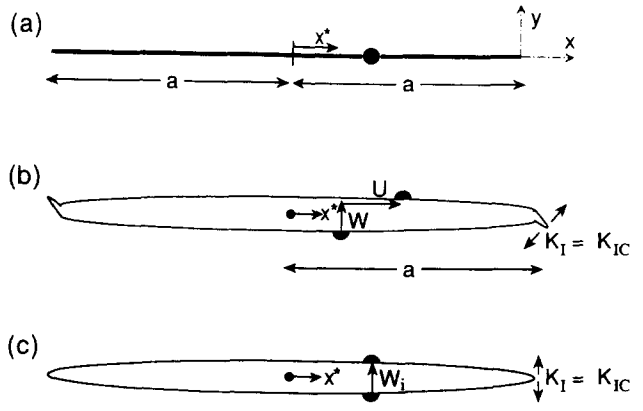

Fig. 9. Definitions of kinematic properties of a crack. (a) Crack length is $2a$. y-co-ordinate normal to crack, x^*- and x-co-ordinates parallel. Dot is a material particle split by the crack. (b) Displacement components, U and W, of part of a material point along a crack wall relative to the other part of the material point along the opposite crack wall. Mode I stress intensity equal to critical stress intensity for mode I fracturing at the time a kink forms. (c) Displacement in mode I loading at the time the initial fracture formed. Material point split and parts displaced only normally relative to one another. Mode I stress intensity equal to critical stress intensity at the time the fracture stops lengthening.

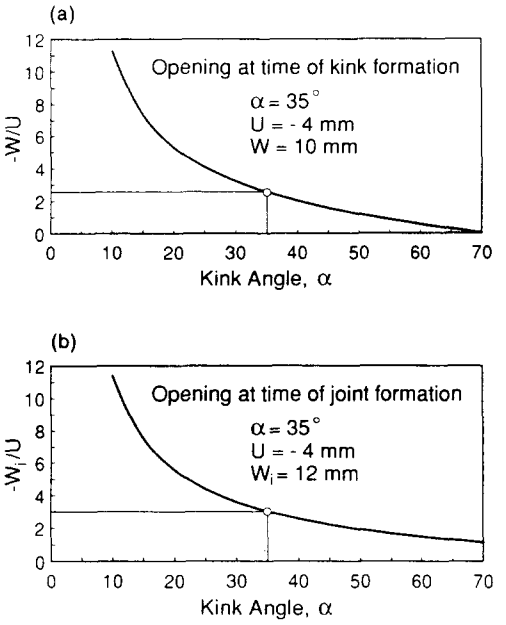

Fig. 10. (a) Relation between kink angle and ratio of opening, W, to slip, U (Fig. 9b) along fracture. (b) Relation between kink angle and ratio of initial opening, W_i (Fig. 9c), to subsequent slip, U, along fracture.

of the joint at any position, x^*, measured from mid-length is (e.g. Pollard & Segall 1987, p. 300)

$$W = 2(\sigma_{yy} + p)\left(\frac{1-\nu}{\mu}\right)\sqrt{a^2 - x^{*2}} \qquad (4a)$$

and the amount of displacment, U, across the faulted joint is

$$U = 2\sigma_{xy}\left(\frac{1-\nu}{\mu}\right)\sqrt{a^2 - x^{*2}} \qquad (4b)$$

in which ν is Poisson's ratio and μ is shear modulus.

Examining equations (4a) and (4b) we note that, if we know the ratio of stresses, we know the ratio of displacements along a faulted joint, regardless of the position, x^*, along the fracture:

$$\frac{U}{W} = \frac{\sigma_{xy}}{\sigma_{yy} + p}. \qquad (4c)$$

According to our calculations (result A, above), the stress ratio for the kinked, faulted joint shown in Fig. 5 was about -0.4, so, according to equation (4c),

$$\frac{U}{W} \approx -0.4.$$

Alternatively, we can read the result directly from Fig. 10(a), using the kink angle. The kink angle is 35°, so Fig. 10(a) indicates that the slip ratio is $-W/U = 2.5$.

The slip U along the faulted joint at a point where a narrow zone of deformation bands crosses (Fig. 5) is about -4 mm, so the slip at the time of faulting was at least that large. Thus assuming that, at the time of faulting, $U \approx -4$ mm, then

$$W \approx 10\text{ mm}. \qquad \text{(Result D)}$$

This result indicates that the opening at that point along the joint was positive and about 1 cm wide when the joint slipped. (We show below that the joint was only slightly wider when it formed than when it kinked.)

Moab Rule of opening widths of kinked joints

According to the Moab Rule, which we will derive below, the opening width of a joint at the time the joint formed in mode I loading was greater than or roughly equal to the amount of slip across the faulted joint at the time it kinked in response to mode II loading.

The derivation of the Moab Rule is motivated by the observation that kinked joints in the Garden Area have slipped a few mm or a few cm, and the assumptions that the amount of slip should be related to the regional shear stress required to cause a kink to form at the end of the joints, and that the amount of shear stress should be related to the mode I fracture toughness of the rock. Other key assumptions are that the fracture toughness was the same at the times the joints and kinks formed, and that the amount of slip at the time the kinks formed is currently recorded in the offset of markers along the faulted joints. This method will work only where a kinked tail crack occurs, because it assumes that the stress intensity at the end of a pupative tail crack was equal to the fracture toughness. Even if the history of the fracture has been so simple that it has slipped only once, the observed slip should underestimate the amount of slip at the time the joints faulted, because part of the slip probably was recovered elastically. Nevertheless, in these cases, the Moab Rule should provide a lower-bound estimate of the amount of mode I opening.

The derivation is as follows. The stress-intensity factor for a pupative fracture growing from the end of a joint subjected to mode I and mode II loading (Fig. 9b) is given by equation (1a). If the stress-intensity factor is

equal to the critical value, K_{IC} (Atkinson & Meredith 1987), then equation (1a) can be written as,

$$\frac{K_{IC}}{k_{II}} = \frac{1}{4}\frac{k_I}{k_{II}}[3\cos(\alpha/2) + \cos(3\alpha/2)] - \tfrac{3}{4}[\sin(\alpha/2) + \sin(3\alpha/2)]. \quad (5a)$$

At the time the joint formed, the width, W_i, of the joint (Fig. 9c) at any position, x^*, is given by equation (4a). However, the stress was critical for propagation, so the width at the time the joint propagated to its final length, a, was

$$W_i = \frac{2K_{IC}}{\sqrt{\pi a}}\left(\frac{1-\nu}{\mu}\right)\sqrt{a^2 - x^{*2}}. \quad (5b)$$

Later on (Fig. 9b), the amount of displacment, U, across the faulted joint was

$$U = \frac{2k_{II}}{\sqrt{\pi a}}\left(\frac{1-\nu}{\mu}\right)\sqrt{a^2 - x^{*2}} \quad (5c)$$

in which ν is Poisson's ratio and μ is shear modulus.

Combining equations (5b) and (5c)

$$\frac{K_{IC}}{k_{II}} = \frac{W_i}{U}$$

and substituting into equation (5a), we derive an expression for the ratio of the initial width, W_i, of the joint when it formed and the faulting displacement, U, across the joint when it kinked:

$$\frac{W_i}{U} = \frac{1}{4}\frac{k_I}{k_{II}}[3\cos(\alpha/2) + \cos(3\alpha/2)] - \tfrac{3}{4}[\sin(\alpha/2) + \sin(3\alpha/2)]. \quad (6a)$$

We note that the width, W_i, and displacement, U, can be determined at any point along the faulted joint, but they must be determined at the same point.

Equation (6a) is solved in combination with equation (1b) in order to determine the displacement ratio, W_i/U, as a function of kink angle, α. The general relation is shown in Table 1 and Fig. 10(b).

A useful extreme that is easy to remember is the ratio of displacements where a joint was faulted by being subjected to pure, mode II deformation. In that case equation (6a) becomes,

$$\frac{W_i}{U} = -\tfrac{3}{4}[\sin(\alpha/2) + \sin(3\alpha/2)]; \quad k_I = 0 \quad (6b)$$

$$\frac{k_I}{k_{II}} = 0; \quad \alpha \approx -70.5°$$

so that

$$\frac{W_i}{U} \approx 1.15. \quad (6c)$$

This yields the Moab Rule: *The width, W_i, of the joint at the time it formed under mode I loading* (Fig. 9c) *was greater than or roughly equal to the displacment, U, at the time the joint faulted and became kinked* (Fig. 9c).

Examining once more the two long joints shown in Fig. 5, the lower joint is offset about 4 mm in a left-lateral sense within about 1.5 m of its northern end. The lower faulted joint has a kinked tail crack at its northern end, so, according to the Moab Rule, we would estimate that the joint had a width of at least 4 mm at the time it formed.

The kink angle of the tail crack is +35°, so, according to Table 1 and Fig. 10(b), the displacement ratio is $W_i/U = -3$, and the more refined estimate would be that the joint was open about 12 mm at the time it formed in mode I.

We estimated in result D that the joint was open about 10 mm when it kinked in mode I and mode II, so the mode I loading changed only slightly at the time the joint kinked, as compared to the time it formed.

The upper fracture shown in Fig. 5 is offset in a left-lateral sense at a position about three m from its south end, where there is a series of kink-like, horsetail cracks. The fracture has been offset about 1 cm, and the kink angle of the tail fractures is again about +35°, so we would estimate that the joint at that point was open about 3 cm at the time it formed.

Curved kinks

Cottrell & Rice (1980) also investigated effects of the full, two-dimensional stress state on the propagation paths of fractures, including effects of compression parallel to the trace of the fracture. According to linear fracture mechanics, this stress has no effect on fracturing. Cottrell and Rice show that the change in orientation of a small, kinked extension of a straight crack is determined by the magnitudes of all components of the stress field.

If x and y are co-ordinates with origin at the tip of the crack, and L is a characteristic length, then the slope of the kinked crack is (Cottrell & Rice 1980, equation 44)

$$\frac{dy}{dx} = \alpha_0 e^{x/L}\,\mathrm{erfc}(-\sqrt{x/L}) \quad (7a)$$

in which the kink angle is

$$\alpha_0 = -2\frac{k_{II}}{k_I} = -\frac{2\sigma_{xy}}{\sigma_{yy} + p} \quad (7b)$$

and the square root of the characteristic length is

$$\pm\sqrt{L} = \sqrt{\frac{a\pi}{8}\left(\frac{\sigma_{yy} + p}{\sigma_{yy} - \sigma_{xx}}\right)}. \quad (7c)$$

The sign of the square root of the characteristic length in equation (7c) is a shape parameter that we will discuss below, and is determined by the sign of the denominator. The characteristic length is the x-distance over which the slope of the tail crack increases by a factor of five (if $\sqrt{L}$ is negative) and decreases by a factor of about two (if $\sqrt{L}$ is positive). It is expressed in units of the half-length, a, of the crack.

In order for these results to be valid, (x/L) and (k_{II}/k_I) must be small, and $(\sigma_{yy} + p)$ must be positive. The shape

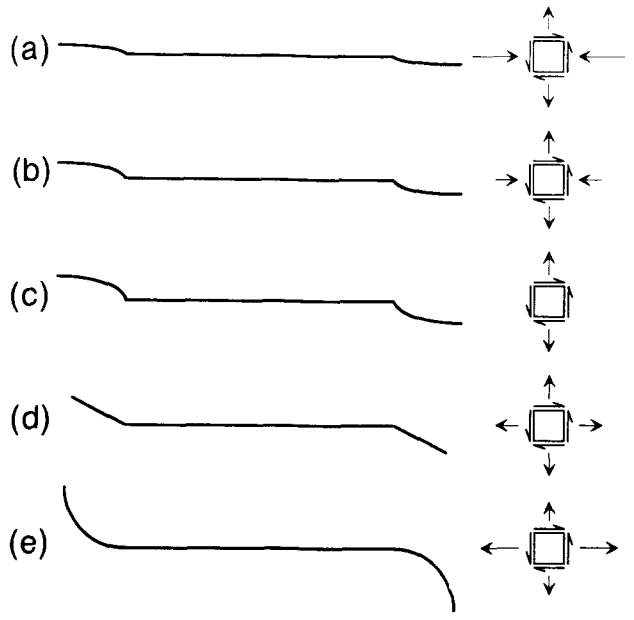

Fig. 11. Examples of idealized curved tail cracks for various far-field loading conditions. In all cases, pressure within the fracture is adjusted to cause propagation. In (a) & (b), the stress parallel to the fracture is compressive and in (c) it is zero. Tail cracks kink and then converge. In (d) the stress parallel to the fracture is tensile and equal to that normal to the fracture. The fracture merely kinks. In (e), the stress parallel to the fracture is a larger tensile stress than that normal to the fracture, and the tail crack diverges.

of the tail crack is determined by integrating equation (7a):

$$y = L\alpha_0 [e^{x/L} \operatorname{erfc}(-\sqrt{x/L}) - 1 - 2\sqrt{x/\pi L}]. \quad (8)$$

Equation (8) indicates that all the essential information about the shape of an isolated tail crack is contained in two variables—the initial kink angle, α_0, and the characteristic length, L—actually the square root of the characteristic length, equation (7c).

Figure 11 shows five hypothetical examples of tail cracks formed under a variety of loading conditions. In all examples the far-field normal stress, σ_{yy}, is a constant tension. The shear stress is positive, so the kink angle is always negative, equation (7b). The primary variable of interest is the far-field normal stress, σ_{xx}, parallel to the crack. It ranges from high compression (Fig. 11a) to high tension (Fig. 11e). In each case, the crack is subjected to pressure, p, sufficient, in combination with the far-field normal stress, σ_{yy}, for the stress intensity at the crack tip to equal the fracture toughness of the rock, assumed here to be a constant.

The essential difference between the first two examples, Figs. 11(a) & (b), is the convergence of the tail crack: the path of the tail crack markedly converges toward the path of the main crack where the far-field stress, σ_{xx}, parallel to the crack is a large compressive stress (Fig. 11a). The path of the tail crack converges less abruptly if the compression is reduced (Fig. 11b) or becomes zero (Fig. 11c). If the far-field stress parallel to the crack is a small tensile stress, the path still converges, but more gradually, and if the stresses normal and parallel to the main crack are equal tensions, the path remains a straight kink (Fig. 11d). The path of the tail

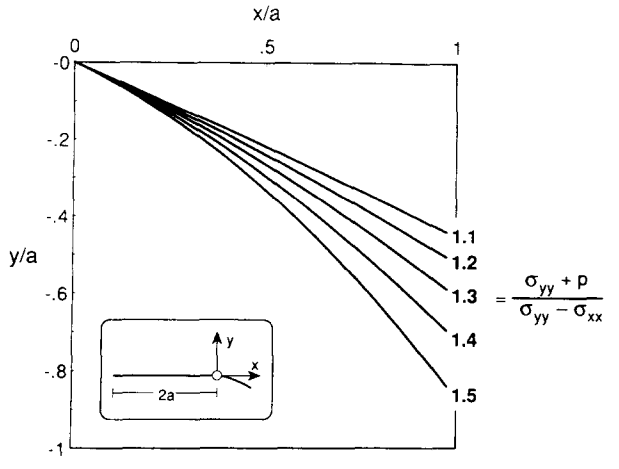

Fig. 12. A family of divergent tail cracks. The kink angle is −22°, reflecting positive (right-lateral) shear.

crack diverges if the far-field tension parallel to the crack is greater than the far-field tension normal to the main crack (Fig. 11e).

The shape of a family of tail cracks, all initiating at a kink angle of −22°, is shown in Fig. 12. Besides the kink angle, which is determined by the shear-stress ratio, $\sigma_{xy}/(\sigma_{yy} + p)$, the shape of each tail crack is determined by the stress-difference ratio, $(\sigma_{yy} - \sigma_{xx})/(\sigma_{yy} + p)$. Figure 13 shows forms of convergent cracks for stress-difference ratios ranging from 0.5 to −2.0, and for lengths of tail cracks ranging from one-tenth to one times the length of the crack itself. The figure shows that the convergence becomes more obvious as the tail crack lengthens to become a major fraction of the original crack and as the stress-difference ratio becomes a large negative number. The figure shows that the curvature of the convergent crack is insensitive to the stress-difference ratio.

Thus these results provide one further important piece of information about the shape of a tail crack:

(4) The stress parallel to the crack plays a major role in determining the initial deviation in shape of a fracture from an original straight, kinked crack. *The sign of the convergence (or divergence) of the tail crack is determined solely by the sign of the difference between far-field*

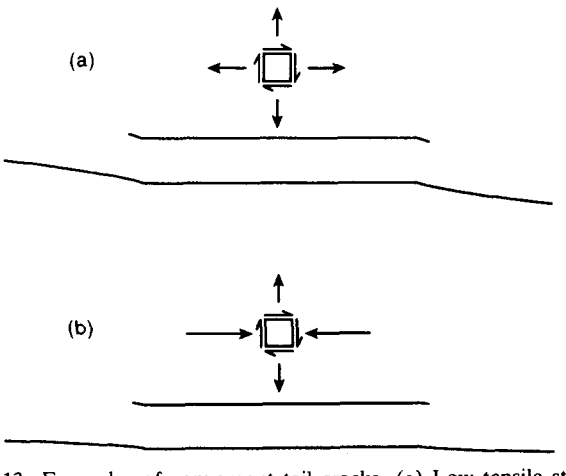

Fig. 13. Examples of convergent tail cracks. (a) Low tensile stress parallel to fracture. (b) Compression parallel to fracture.

normal stresses $[\sigma_{yy} - \sigma_{xx}]$. *The simple rule of thumb is that the tail crack always turns toward the direction of maximum compression (minimum tension).*

All three kinked fractures we have described (Figs. 4 and 5) appear to be neither divergent nor convergent, but rather are straight. All three, though, are short. The kink shown at the northern end of the lower joint in Fig. 5 is about $h = 0.2$ m long, and the joint is more than 10 m long—a is greater than 5 m—so the ratio of h/a is less than 0.04. Although the kink angle for the joints shown in Fig. 12 is 22° (whereas the kink angle for the joint shown in Fig. 5 is 35°), it is clear that for a length, x/a, of 0.04 the kink would be practically straight, regardless of the stress-difference ratio, $(\sigma_{yy} - \sigma_{xx})/(\sigma_{yy} + p)$. One cannot determine the stress-difference ratio by studying the shapes of short kinks such as those shown in Figs. 4 and 5.

HORSETAIL FRACTURES

There are groups of subparallel fractures near the ends of some joints which branch out from the joint something like the hairs in a horse's tail (described along faulted joints in granite by Davies & Pollard 1986). In the Garden Area, there are horsetail fractures up to several metres long near the southwestern ends of many of the J-2 joints that trend about N30°E in the northern and southern parts of the Garden Area (Fig. 2). Figure 14(a) shows horsetail fractures, 1–10 dm long, on the left side of a faulted joint in Entrada Sandstone that terminates in an echelon joint set just beyond the plastic scale card. The horsetail fractures branch off in a counterclockwise sense, at an angle of 60–70°.

Other cracks of the horsetail type are shown in the map in Fig. 16, stations 29 m and 35 m. The cracks generally connect the two adjacent joints. Here the offset of band faults indicates right-lateral shearing, and the joints step right, so the secondary, horsetail cracks occur where one would expect tension near the end of the host fractures.

Echelon cracks also occur near the ends of some joints and might be confused with horsetail fractures. Comparison of the horsetail fractures at stations 29 m and 35 m with the echelon cracks at station 13 m in Fig. 16 indicates, however, that they are different structures. The traces of the echelon cracks are unconnected to the host fracture, whereas the traces of the horsetail fractures are connected.

Thus, horsetail fractures occur on one side or the other in the terminal regions of a host fracture. They are cracks that apparently have initiated at irregularities along a slipping host fracture and occur where tension is developed as a result of slip along the host fracture.

The location of the horsetail fractures shown in Figs. 14(a) and 16 suggests that they formed in the area along the faulted joint where the rock was subjected to tension at the time the joint slipped. A counterproof of this argument is that the horsetail fractures are absent from the side of the faulted joint where the rock was subjected to compression when the joint slipped. Horsetail fractures apparently initiate at roughness elements along the surface of a joint and the direction of crack propagation is normal to the direction of maximum tension. Thus the sense of slip is deduced in the same way for single kink cracks and for multiple horsetail fractures. Unlike the kink cracks, though, we can determine only the direction of maximum tension by examining the fractures. The primary values in recognizing horsetail fractures are that they indicate the location where slip is ending along a host fracture, the sense of faulting accommodated by the host fracture, and the direction of maximum tension (Davies & Pollard 1986).

Cracks that are closely related to horsetail fractures occur in the northern and southern parts of the Garden Area along host, faulted joints that trend N30°E (Fig. 2). These cracks are roughly parallel to the horsetail fractures, but they occur anywhere along the host joints. The cracks occur on either side of the host, but never cut across the host. Like horsetail fractures and bridge fractures (Davies & Pollard 1986, Martel *et al.* 1988), these cracks apparently are a result of a combination of slip along a rough fault and overall tension, in this case in an E–W direction. Roughness elements apparently act as nuclei for the cracks.

OVERLAPPING AND VEERING OF FRACTURES

Most of the joints that we have examined in the Garden Area occur nearby others, so the stress state responsible for crack propagation will change as the cracks interact. Two manifestations of changing stress fields are overlapping fractures and veering fractures.

Traces of many of the joints in the Garden Area overlap for distances that are great in comparison to the separation of the joints. For example, joints shown in Fig. 16, at station 5 m, overlap 3–4 m and are separated 0.05–0.08 m, so the overlap is 10–20 times the separation. The two long joints shown in Fig. 16 have an overlap that is 10–12 times the separation. The traces are virtually parallel.

The traces of joints shown in Fig. 14(b) are many meters long and overlap about 1.5 m, whereas they are separated only about 0.05 m. The joint on the left is practically straight in the overlap area, but it kinks abruptly about 15° clockwise near its tip. The joint on the right is straight to approximately the tip of the joint on the left, veers gently toward it, and then straightens out to become parallel with it.

Examples of veers are shown in Fig. 15(a).The veers are at station 67 m in the map in Fig. 17. Another example of a veer is shown at station 32.5, Fig. 16. Figure 15(a) shows the ends of two joints overlapping about 10 dm and right-stepping about 1 dm. The tip of the joint on the right veers smoothly but curves tightly over a horizontal distance of about 2 dm toward the joint on the left and terminates about 0.5 dm from it. The joint on the left veers openly toward the joint on the right over a horizontal distance of about 5 dm.

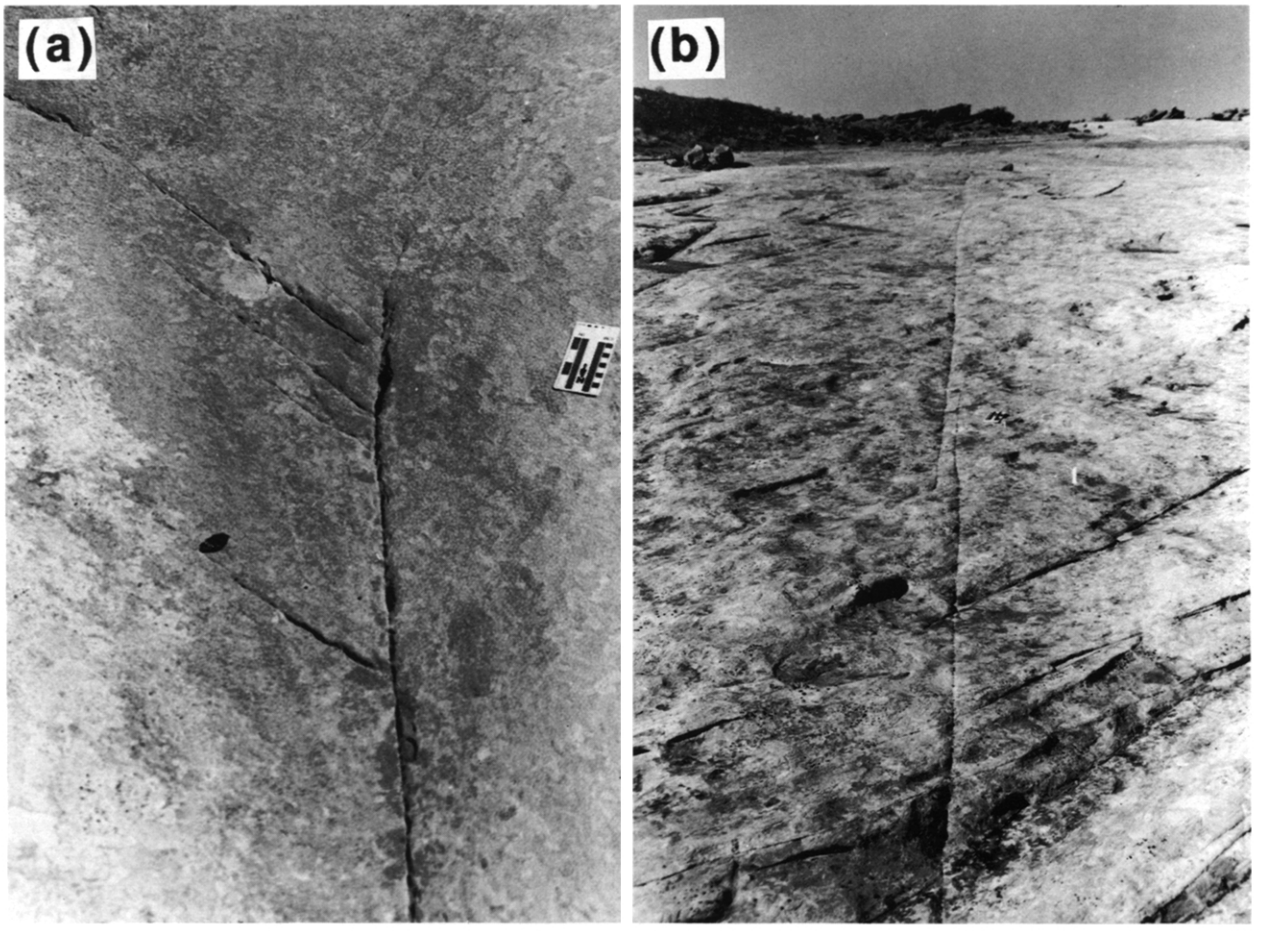

Fig. 14. (a) Example of horsetail factures at end of a faulted joint (left-lateral shear). (b) The traces of joints shown here are many meters long and overlap about 1.5 m, whereas they are separated only about 0.05 m.

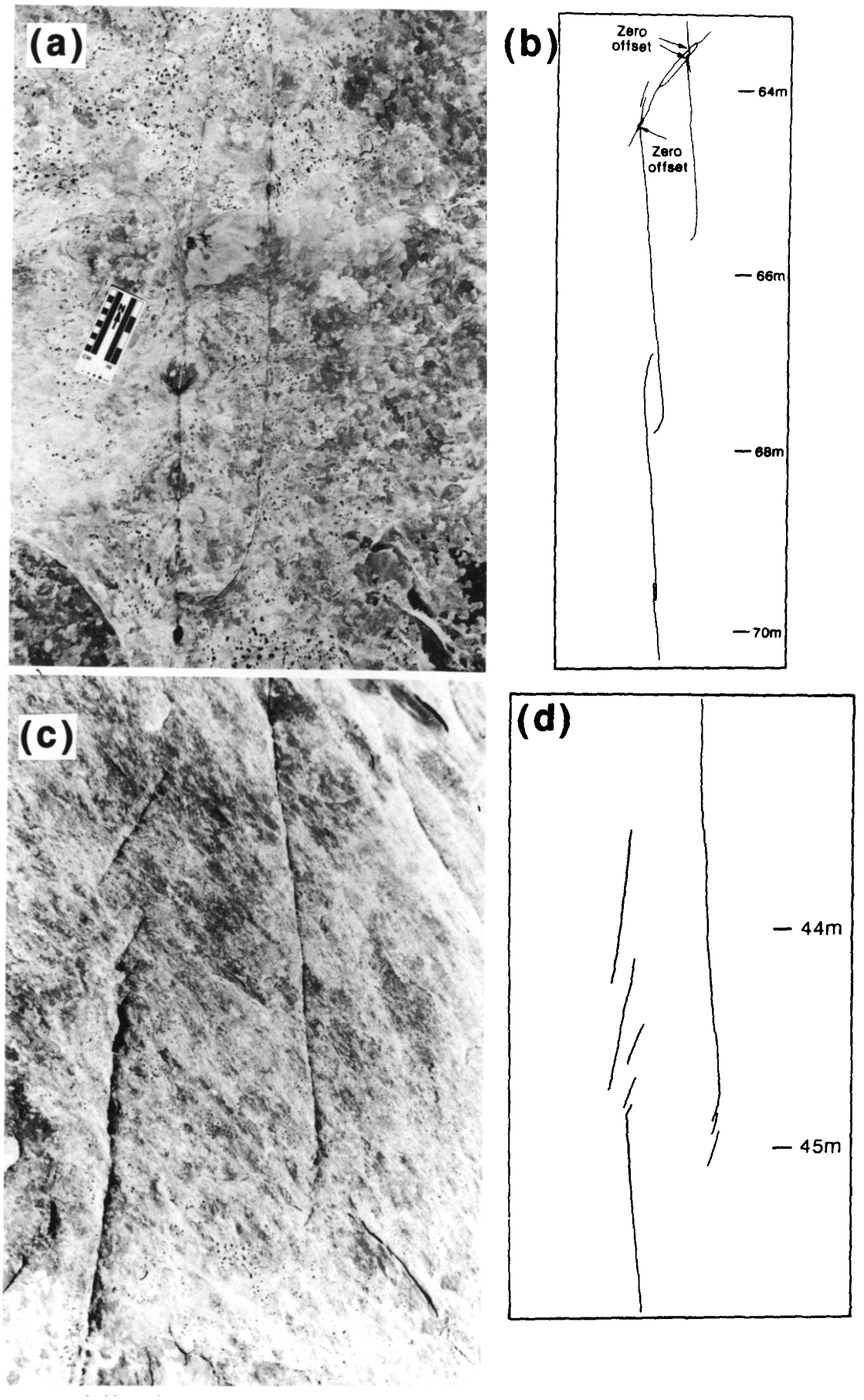

Fig. 15. Examples of veers. (a) Photograph of overlapping joint segments. The ends of two joints overlap about 10 dm and right-step about 1 dm. (b) Map showing overlapped joint segments at station 67.5 m. (c) & (d) Map and photograph of echelon cracks at the tips of overlapping joint segments at station 45 m (Fig. 17). The echelon cracks range in length from a few cm to about 1 m.

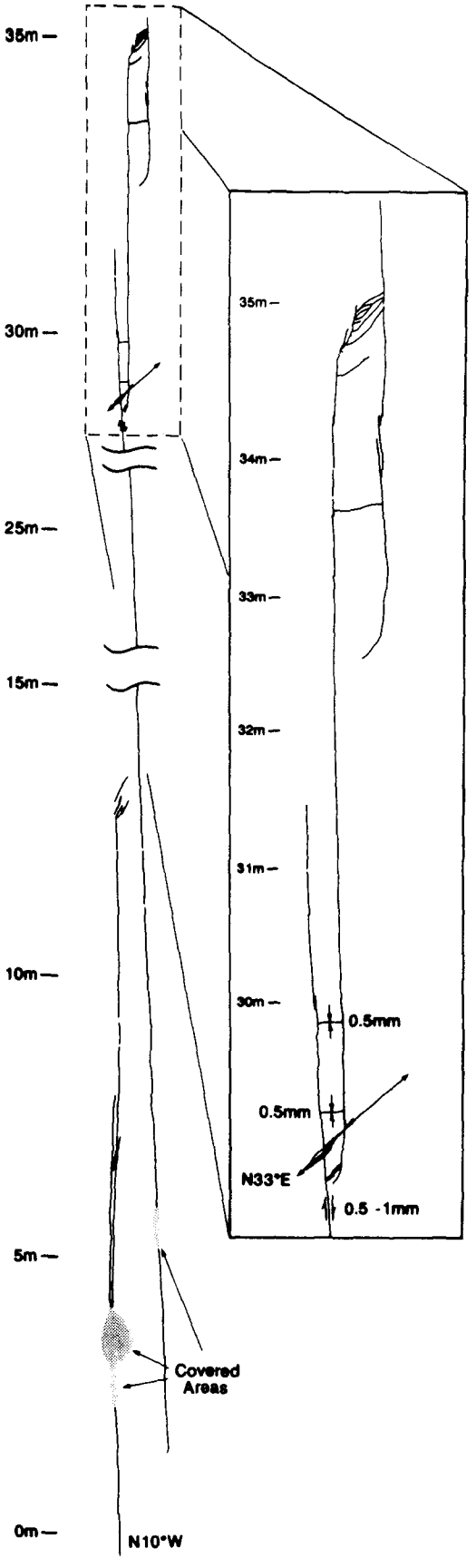

Fig. 16. Horsetail fractures, bridge cracks and echelon cracks along faulted joints near coordinate 1100N 750E (Fig. 2) in the Garden Area. Horsetail fractures at stations 28 m and 35 m. Bridge cracks at stations 29 m, 29.8 m and 33.5 m. Echelon cracks at 13 m. The sense of slip is right-lateral, and the amount of slip is 0.5–1 mm near station 28.5 m.

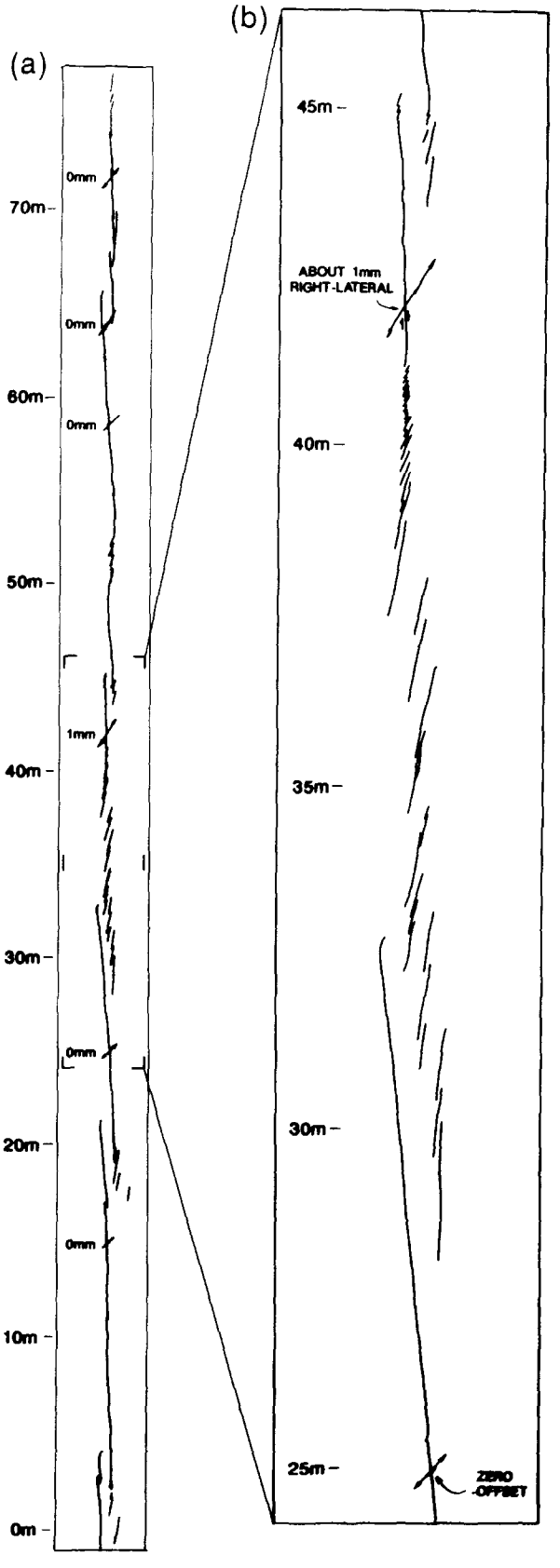

Fig. 17. Stepping joint segments and echelon cracks in part of the Garden Area where joints have not become faulted. At the scale of (a), the most striking features of the traces of the joint segments are that individual joint segments range in length from 3 to 15 m, and that they are straight but misaligned. The detailed map in (b) indicates two ways that joint segments terminate in the vicinity of neighboring joints. Tips of a segment may simply veer toward a neighbor. Or, beyond the tips of a segment may be a series of echelon cracks. The segments within the zoned joint step right and are twisted a few degrees counterclockwise relative to the trend of the zoned joint, whereas the echelon cracks associated with the segments step left and are twisted a few degrees clockwise relative to the trend of the segment.

One crack veering toward another is unremarkable because cracks interact and generally propagate toward one another (e.g. Pollard & Holzhausen 1979, Delaney & Pollard 1981, Pollard & Aydin 1984, 1988), and the sense of veering can be understood in terms of the Cottrell & Rice (1980) analysis of kinking. Veering, however, is different from kinking primarily because it is gradual.

The overlapping of essentially straight joints is a remarkable phenomenon because it does not appear that the joints were interacting.

Mechanically, though, veering and overlapping can be understood only in terms of stress gradients. Here we will investigate conditions under which interacting cracks can curve strongly or weakly as their crack tips pass. Although the analysis of the effect of stress state on the shapes of propagating fractures by Cottrell & Rice (1980) does not include effects of stress gradients, such as those that occur where two fractures are interacting, we can estimate effects of stress gradients by means of an analysis by Sumi *et al.* (1985), who have extended the analysis of Cottrell and Rice to include effects of gradients of mode I and mode II stress-intensity factors. The extended analysis is useful where cracks are growing within a non-uniform stress field, or where there is a boundary nearby, or where two fractures are interacting.

Expanding the solution by Cottrell & Rice, equation (8),

$$y = \alpha_0 L\left[\frac{x}{L} + \tfrac{4}{3}\sqrt{1/\pi}\left(\frac{x}{L}\right)^{3/2} + \frac{1}{2}\left(\frac{x}{L}\right)^2 + \cdots\right]. \quad (9a)$$

Sumi *et al.* (1985) rewrote the solution as,

$$y = \alpha_0 L\left[\frac{x}{L} + \tfrac{4}{3}\sqrt{1/\pi}\left(\frac{x}{L}\right)^{3/2} + \tfrac{1}{2}(\lambda L + 1)\left(\frac{x}{L}\right)^2\right] \quad (9b)$$

in which parameter λ is to be selected to match boundary conditions. They determined that (*op. cit.*, equation 2.22)

$$\lambda = \frac{1}{k_I}\frac{\partial k_I}{\partial h} + \frac{1}{k_{II}}\frac{\partial k_{II}}{\partial h} \quad (9c)$$

in which h is the length of the tail crack in the x-direction. The significance of the modification of the solution is most apparent if one examines curvature which, according to equation (9b), is

$$\frac{d^2y}{dx^2} = \frac{\alpha_0}{L}\left(1 + \sqrt{\frac{L}{\pi x}}\right) + \lambda\alpha_0. \quad (10a)$$

Substituting equations (9c) into this result,

$$\frac{d^2y}{dx^2} = \frac{\alpha_0}{L}\left(1 + \sqrt{\frac{L}{\pi x}}\right) + \frac{\alpha_0}{k_I}\frac{\partial k_I}{\partial h} - \frac{2}{k_I}\frac{\partial k_{II}}{\partial h}. \quad (10b)$$

According to equation (10a), the curvature of a crack is determined not only by the kink angle and the characteristic length, but also by the gradients of the stress field through the parameter λ. The characteristic length, through the sign and magnitude of $\sqrt{L}$, is determined by the stress state, equation (7c). Thus, if λ is sufficiently large and opposite in sign from $\sqrt{L}$, a tail crack can first curve one way, inflect, and then curve the other way (Sumi *et al.* 1985). In this manner Sumi *et al.* (1985) show that the spatial gradients of stress, which determine spatial gradients of the stress-intensity factors, also cause a crack to curve as it propagates. Furthermore, a crack can veer smoothly, without kinking, as a result of a gradient in shear stress, as indicated in equation (10b) by setting the kink angle equal to zero:

$$\frac{d^2y}{dx^2} = -\frac{2}{k_I}\frac{\partial k_{II}}{\partial h}; \quad \alpha_0 = 0. \quad (10c)$$

(5) *If the fracture veers in a smooth curve, rather than a kink, the shear stress affecting crack growth was zero as the fracture started to grow and increased as the fracture propagated.*

In computing the gradients of stress intensity factors required in equations (10), we use the solution by Tada *et al.* (1985, p. 5.12) for stress-intensity factors derived for a crack subjected to boundary tractions, T:

$$\begin{pmatrix} k_I \\ k_{II} \end{pmatrix} = \begin{pmatrix} T_y \\ T_x \end{pmatrix}\sqrt{\pi/a}\,[\sin^{-1}(c/a) - \sin^{-1}(b/a) \mp \sqrt{1-(c/a)^2} \pm \sqrt{1-(b/a)^2}]. \quad (11a)$$

Equation (11a) is summed for a series of patches on a crack. Here c and b are co-ordinates of the ends of a patch and T_y and T_x are tractions on a patch (details are presented elsewhere by Cruikshank 1991). Our method of solving for the interaction of cracks is similar to that of Pollard & Holzhausen (1979).

The stress, σ_{xx}, in equation (7c) is what Cottrell & Rice (1980) refer to as the non-singular part of the expression for horizontal normal stress. For the solution we are using, it is

$$\sigma_{xx} = T_y\frac{1}{\pi}\left[\sin^{-1}\left(\frac{a^2 - cx}{ax - ac}\right) - \sin^{-1}\left(\frac{a^2 - bx}{ax - ab}\right)\right] \quad (11b)$$

in the limit as x approaches a.

Figure 18 shows mode I and mode II stress-intensity factors for two interacting cracks as a function of horizontal spacing of crack tips and for a vertical spacing of crack tips of $0.1a$. The four curves in Fig. 18 represent mode I and mode II stress-intensity factors for the positive (right) and negative (left) ends of the left crack. The mode I stress-intensity factor increases to a maximum of about 2.6 times the stress-intensity factor for an isolated crack as the crack tips begin to overlap, then decreases markedly thereafter. It is less than that for an isolated crack when the tips overlap more than about $0.25a$ (tip spacing of $-0.25a$). Indeed, the positive end would stop propagating when the overlap was about $0.2a$ because, for greater overlap, the stress-intensity factor is greater at the negative than the positive end of the left crack (Fig. 18).

The mode II stress-intensity factor, which controls the direction of kinking and largely controls the curvature, is

a small positive value, so that the two cracks would tend to diverge where the tip spacing is greater than about $0.1a$. For smaller tip spacing and for overlap, the mode II factor is negative, so the cracks will tend to converge (Fig. 18).

Figure 19 shows approximate forms of short extensions of interacting, mode I cracks, as a function of tip spacing. The body containing the cracks was subjected to far-field normal stresses parallel and normal to the cracks and to zero far-field shear, and the shape of the short extensions were derived according to equation (9b). In each case the two initial cracks were straight, and their trends were offset by $0.1a$. The curvature of the extensions reflect the local stress fields generated around the interacting crack tips as well as the far-field stresses. The several examples in each case are for far-field stress-difference ratios, $(\sigma_{yy} - \sigma_{xx})/(\sigma_{yy} + p)$, ranging from +6 (highly convergent) to −3 (moderately to highly divergent). In each case the curvature due to the gradient in the shear stress in the vicinity of the crack tips is visible in the curves for stress-difference ratios of zero (Fig. 19).

The two examples shown in Figs. 19(a) & (b) are for tip spacings of $0.3a$ and $0.1a$. The results show that, if the far-field normal stresses are equal, $(\sigma_{yy} - \sigma_{xx})/(\sigma_{yy} + p) = 0$, the shear stress due to interaction causes the propagating cracks to curve outward, away from one another, until the tips overlap, and then to curve inward as the tips further overlap (Fig. 19). The results further show that the effect of the stress-difference ratio is entirely as expected. If the stress-difference ratio is moderately to strongly negative, the crack curves strongly outward or inward, depending on the kink angle of the crack. If the stress-difference is strongly positive, the crack tends to turn back toward its original path, prior to kinking.

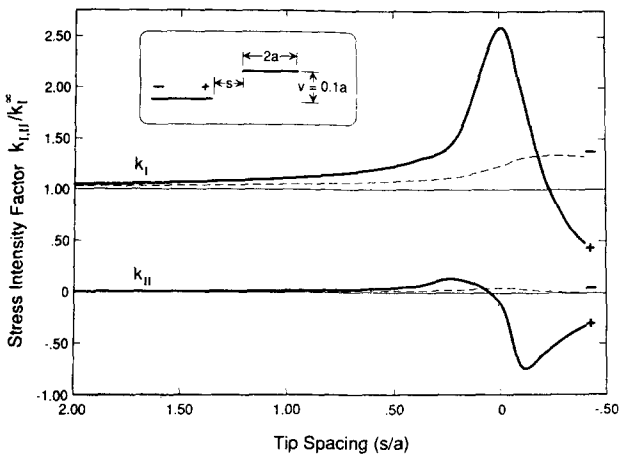

Fig. 18. Mode I and mode II stress-intensity factors for two interacting cracks as a function of horizontal spacing of crack tips and for a vertical spacing of crack tips of $0.1a$. The four curves represent mode I and mode II stress-intensity factors for the positive (right) and negative (left) ends of the left crack. The mode I stress-intensity factor increases to a maximum of about 2.6 times the stress-intensity factor for an isolated crack as the crack tips begin to overlap and then decreases markedly thereafter. The mode II stress-intensity factor, which controls the direction of kinking and largely controls the curvature, is a small positive value, so that the two cracks would tend to diverge where the tip spacing is greater than about $0.1a$. For smaller tip spacing and for overlap, the mode II factor is negative, so the cracks would tend to converge.

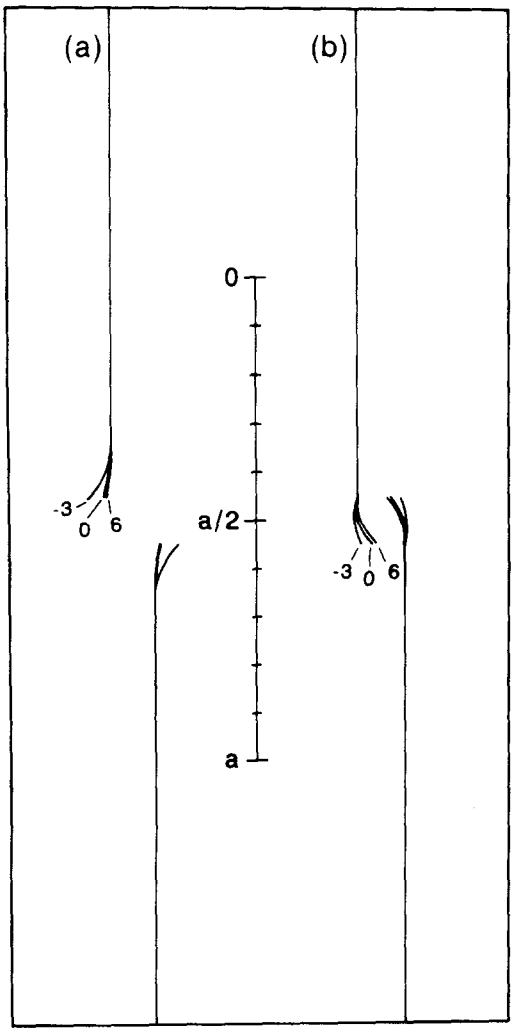

Fig. 19. Approximate forms of short extensions of interacting, mode I cracks, as a function of horizontal tip spacing. The body containing the cracks was subjected to far-field normal stresses parallel and normal to the cracks and to zero far-field shear, and the shape of the short extensions were derived according to equation (9b). In each case the two initial cracks were straight, and were separated by $0.1a$ in the horizontal direction. The curvature of the extensions reflect the local stress fields generated around the interacting crack tips as well as the far-field stresses. The several examples in each case are for far-field stress-difference ratios, $(\sigma_{yy} - \sigma_{xx})/(\sigma_{yy} + p)$, ranging from +6 (highly convergent) to −3 (moderately to highly divergent). In each case, the curvature due to the gradient in the shear stress in the vicinity of the crack tips is visible in the curves for stress-difference ratios of zero.

Olson & Pollard (1988, 1989) have used a boundary-element model to study crack growth and interaction, with essentially the same purpose in mind as we; that is, to study interactions of idealized fractures. Their model includes fixed far-field normal stresses, and fluid pressure is adjusted in the cracks to maintain the mode I stress-intensity factor at the limit, the fracture toughness. Some of their results are given in Fig. 20. In each case, the cracks originally were about 0.5 m long and widely separated. Each crack was allowed to grow at only one end, so the cracks grow only toward one another. The simulation is terminated when the cracks stop propagating toward one another, which is essentially when the driving pressure in the cracks exceeds the

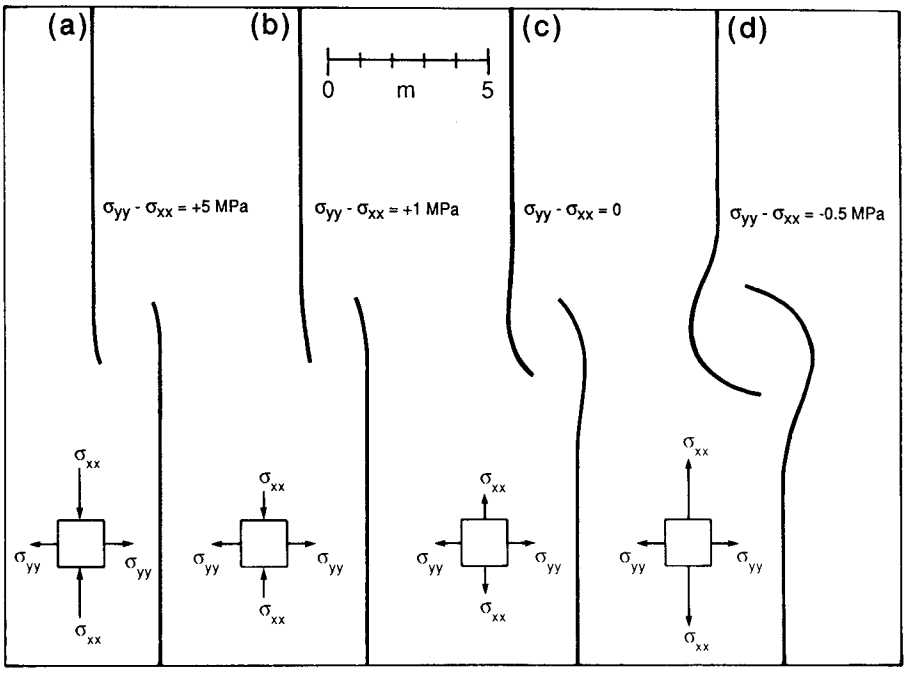

Fig. 20. Interactions of idealized fractures according to Olson & Pollard (1988, 1989). Their model includes fixed far-field normal stresses, and fluid pressure is adjusted in the cracks in order to maintain the mode I stress-intensity factor at the fracture toughness. In each case the cracks originally were about 0.5 m long and widely separated. Each crack was allowed to grow at only one end, so the cracks grow only toward one another. The simulation is terminated when the cracks stop propagating toward one another. Their results show the marked effects of the stress-difference, $\sigma_{yy} - \sigma_{xx}$, on the shapes of interacting cracks.

driving pressure required to propagate an isolated crack. Their results show the marked effects of the stress-difference ratio, $(\sigma_{yy} - \sigma_{xx})/(\sigma_{yy} + p)$, on the shapes of interacting cracks.

In light of these theoretical results, we interpret the overlapped joints shown in Fig. 14(b) as follows. The two joints only weakly interacted. The joint on the left developed before it was close to the joint on the right because its trace is straight. The kink at its tip reflects minor right-lateral shear that occurred when the joints in this area slipped in a right-lateral sense and became faulted joints (this joint is in the vicinity of co-ordinates 1300N, 400E). The kink angle is $-10°$ (minus because it is clockwise, Fig. 7a) so, according to equation (7b),

$$-10°\left(\frac{\pi}{180°}\right) \approx -0.17 \text{ radians} \approx \alpha$$

$$= -2\frac{k_{II}}{k_I} = \frac{-2\sigma_{xy}}{\sigma_{yy} + p}.$$

Thus the shear, mode II stress-intensity factor was about one-tenth the mode I stress-intensity factor. Also, the shear stress was positive (Fig. 8a).

The joint shown on the right in Fig. 14(b) developed after the joint on the left because its trend deviates slightly in the vicinity of the tip of the joint on the left. However, the interaction was slight, apparently reflecting low stress-intensity for the joint on the left at the time the joint on the right formed. Otherwise, the joint on the right would have turned sharply. Furthermore, the joint on the right converged back toward its original trend, indicating that the square root of the characteristic length was both positive and relatively small, so that (equation 7c)

$$(\sigma_{yy} - \sigma_{xx}) > 0$$

and we estimate that

$$\left(\frac{\sigma_{yy} - \sigma_{xx}}{\sigma_{yy} + p}\right) > 1$$

that is,

$$-\sigma_{xx} > p.$$

Thus σ_{xx} was compressive (negative) and greater in magnitude than the pressure in the fracture. The conditions were much as depicted in the simulation shown in Fig. 20(a). This was the condition recognized by Cottrell & Rice (1980) that would cause a crack to continue in its own plane rather than to veer.

In the cases of the overlapping joints shown in Figs. 14(b) and (16), the theory indicates that the compression parallel to the crack was large. Compression parallel to the crack is required for high stability of crack propagation direction, as shown in Fig. 20(a).

The veers (the smoothly but tightly curving fracture terminations shown in Figs. 15b), at 66 m and 67 m in Fig. 17, and at station 32.5 in Fig. 16), reflect a decrease in the stability of propagation direction of the cracks. The negative mode II stress-intensity factor that results from interaction of two overlapping cracks (Fig. 18) will cause the crack tips to veer toward the neighboring crack surfaces unless the compression parallel to the crack is very large. Thus the veering presumably reflects a re-

duction in the compression parallel to the cracks after the cracks had overlapped one another.

STEPPED JOINTS AND ECHELON CRACKS

Examination of intersections of older band faults and younger joints indicates that the joints within the rocks between co-ordinates 1600N 300E and 1400N 700E (Fig. 2) were subjected to negligible shearing subsequent to their formation. Examples are shown in Fig. 17, which shows in more detail the segments of a single zone of joints that occurs between co-ordinates 1500N 350E and 1350N 375E (Fig. 2). The joint segments cross a half-dozen band faults and the largest offset is one mm, so the segments were not sheared subsequently and the pattern of segments presumably appears essentially as it did when the zones of joints formed.

At the scale of Fig. 17(a), the most striking features of the traces of the joint segments are that individual joint segments range in length from 3 to 15 m, and that they are straight but misaligned, forming an echelon pattern. The traces are oriented a few degrees counter-clockwise relative to the trend (about N5°W) of the zone of joints itself, so the joint segments step right.

Studies of jointing by Pollard and others (Pollard 1976, Pollard *et al.* 1982, Segall & Pollard 1983a,b, Pollard & Aydin, 1984, 1988, Segall 1984, Pollard & Segall 1987, Rubin & Pollard 1988) have provided us with a basis for interpreting echelon joints that form at the edge of a parent joint (Fig. 21). The edge of the parent joint is subjected to a combination of mode I and mode III deformation but, rather than twisting as a unit as it propagates, the master joint breaks down into blades which are roughly parallel to the directions of maximum and intermediate compression (Fig. 21) (Pollard *et al.* 1982). Thus we imagine that the small amount of twist of the long joint segments shown in Fig. 17(a) is a result of modest left-lateral shear in combination with dominant, N85E extension.

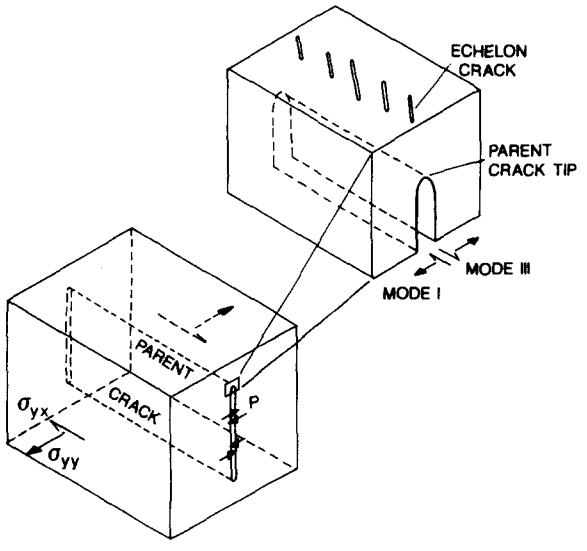

Fig. 21. Conditions responsible for formation of echelon cracks and breakdown of a fracture at its outer edge. The edge of the parent crack is subjected to a combination of mode I and mode III deformation but, rather than twisting as a unit as it propagates, the edge of the parent crack breaks down into blades which are roughly parallel to the directions of maximum and intermediate compression (after Pollard *et al.* 1982).

The size of the area affected by the stress state, determined by studying the segmented joints, should be the size of area where the segmented joints have the same sense of stepping. According to our mapping, the segmented, right-stepping joints occur within an area with dimensions of 100 or 200 m on a side; certainly not throughout the whole Garden Area (Fig. 2).

The map of the segmented, zoned joint shown in Fig. 17 shows two ways that joint segments terminate in the vicinity of neighboring joints: Tips of a segment may simply veer toward a neighbor, or, beyond the tips of a segment may be a series of echelon cracks (Foering 1968, Nicholson & Pollard 1985).

Figure 15(c) is a photograph and Fig. 15(d) a map of an area, near the midlength of the zone of joints shown in Fig. 17, where simple echelon cracks occur at the tips of overlapping segments. The echelon cracks range in length from a few cm to about 1 m. Relative to the traces of segments, the traces of the echelon cracks are misoriented a few degrees, up to perhaps 10° clockwise.The echelon cracks step left (Fig. 17b). Thus, the segments within the zoned joint step right and are twisted a few degrees counter-clockwise relative to the trend of the zoned joint, whereas the echelon cracks associated with the segments step left and are twisted a few degrees clockwise relative to the trend of the segment. Another characteristic of the echelon cracks is that the traces of individual cracks are short near the end of the joint segment and become longer with increasing distance from the end of the joint segment (Fig. 17b). In some cases the zone of echelon cracks is short compared to the length of the joint segment (Fig. 15c), and in others it is long (Fig. 17).

Our model of the echelon cracks is shown in Fig. 22 in map view and in three dimensions. It shows the breakdown of a single, master fracture below into multiple fracture blades above. Thus we infer that the joint segments we observe represent fracture blades. We can understand the orientation of the segments by working with a two-dimensional mechanical model of interacting fractures (Fig. 23). One joint has broken through to the surface and has a vertical fracture front. The other is migrating toward the surface and has a horizontal fracture front. The environment of shear stress created in the vicinity of the fracture front of the first joint is shown in Fig. 23(a). In addition to the far-field mode I loading, it is this shear stress that is responsible for the combination of mode I and mode III loading of the second joint, the one that is growing vertically upward. We note that, depending on the sense of stepping of the two joints, the fracture blades will be twisted in a clockwise or a counterclockwise sense (Fig. 24). Comparison of Figs. 15(c) and 24 shows that, for overlapping joint segments that step right, the sense of twist observed in

the echelon cracks is consistent with the sense of twist predicted from analysis of interacting joint segments.

According to Pollard *et al.* (1982), who analyzed the conditions of formation of echelon cracks in front of a rectilinear crack front and the degeneration of a rectilinear crack front into a series of echelon crack blades, the twist angle, β, that a pupative echelon crack blade makes with the trend of the front of the host crack is given by (*op. cit.*, p. 1294, equation 3)

$$\tan(2\beta) = \frac{2}{1-2\nu}\frac{k_{III}}{k_I} \tag{12a}$$

that is,

$$\tan(2\beta) = \frac{2}{1-2\nu}\frac{\sigma_{xy}}{\sigma_{yy}+p}. \tag{12b}$$

The fundamental assumption is that the twisted blade is normal to the direction of maximum tension immediately ahead of the crack front. Equation (12b) is plotted in Fig. 7(b), where the twist angle can be compared to the kink angle. The differences between twists and kinks are shown in Fig. 25.

We can compare expressions for the twist angle resulting from a combination of mode I and III loading with the kink angle resulting from a combination of mode I and mode II loading if we simplify equations (12) for small values of shear stress,

$$\beta \approx \frac{1}{1-2\nu}\frac{\sigma_{xy}}{\sigma_{yy}+p}; \quad \text{twist angle} \tag{12c}$$

and

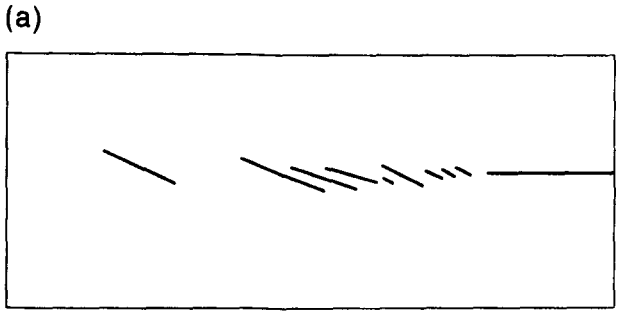

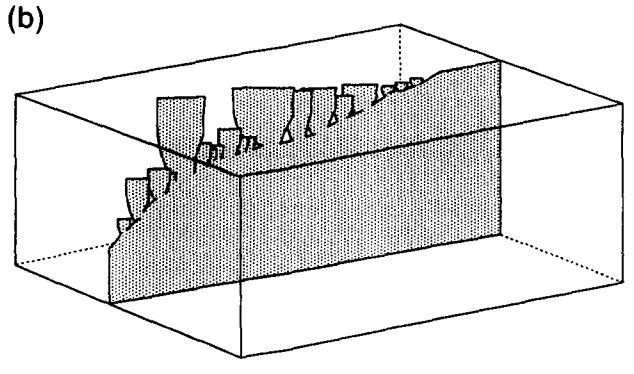

Fig. 22. Map and block diagram of idealized echelon cracks in front of trace of joint, showing how cracks probably twist and connect to parent joint at depth.

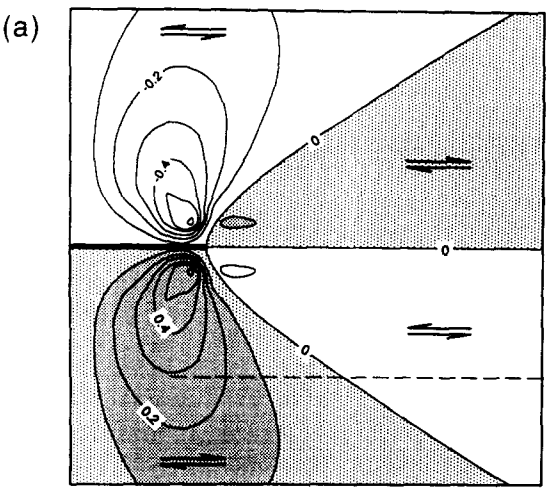

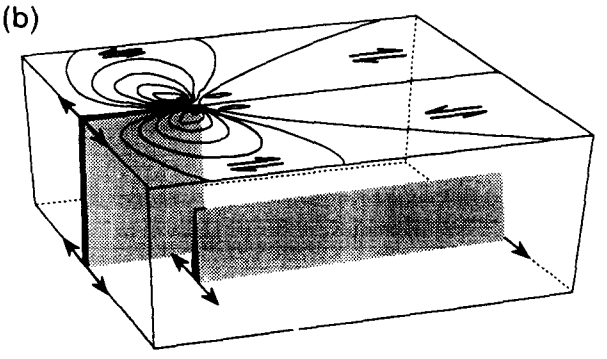

Fig. 23. Map and block diagram of stress state and geometry responsible for formation of echelon cracks. One joint has broken through to the surface and has a vertical fracture front. The shear stresses generated around its tip are shown with contours. The other joint is migrating upward toward the surface and has a horizontal fracture front. It is subjected to far-field mode I loading as well as the shear stress generated around the tip of the first joint. Thus the rising joint is subjected to a combination of mode I and mode III loading.

$$\alpha \approx \frac{-2\sigma_{xy}}{\sigma_{yy}+p}; \quad \text{kink angle (from equation 3b).}$$

Suppose the shear stress, σ_{xy}, is the same. Then the twist angle and the kink angle would be the same, except for the sign, for a Poisson's ratio of 0.25. For highly compressible materials, $\nu = 0$ the twist angle is half the kink angle. For incompressible materials, $\nu = 0.5$, the twist angle is large and is always 45°.

Thus we can understand the geometry of the echelon cracks in the Garden Area with the two-dimensional model, if we bear in mind that the joint segments are three-dimensional fractures. In two-dimensional analysis of the formation of the echelon cracks, we assume that the joint front plunges at a low angle to the outcrop surface (Fig. 22), and consider interaction between joint segments.

The echelon cracks shown in Fig. 15(d), at station 19 m (Fig. 17a) and the longer echelon cracks shown in Fig. 17(b) are twisted at angles ranging from 10° to 20°. If we assume a Poisson's ratio of 0.25 for the sandstone, the shear stress ratio is

$$\frac{\sigma_{xy}}{\sigma_{yy}+p} = \frac{\tan(2\beta)}{4}$$

or

$$\approx -0.1 \text{ to } -0.2. \qquad \text{(Result E)}$$

In this way we can understand how, at one scale, segments of a zoned joint can be subjected to left-lateral shear and, at another scale, the same segments can interact to produce local right-lateral shear, creating the stress environment within which echelon cracks form. It also seems clear that neither the right-lateral shear responsible for the echelon cracks between joint segments in a zone nor the left-lateral shear responsible for the stepping of segments themselves is a regional phenomenon. In order for one to recognize regional causes in a pattern of joints, one must understand and then filter out the local causes in the pattern.

CONCLUDING REMARKS

A wide variety of minor cracks ornament joints that occur within long narrow zones in white Entrada Sandstone in the Garden Area of Arches National Park. In most places the joints accommodated shearing offsets of a few mm to perhaps a dm, and thus became faulted joints, indicating that part of the decoration of minor cracks is due to faulting. However, in a few places, the shearing was zero, so one can examine minor cracks due solely to interaction of joint segments at the time they formed. By applying elementary principles of fracture mechanics to an analysis of the minor cracks, we have been able to infer the conditions under which most of the minor cracks formed.

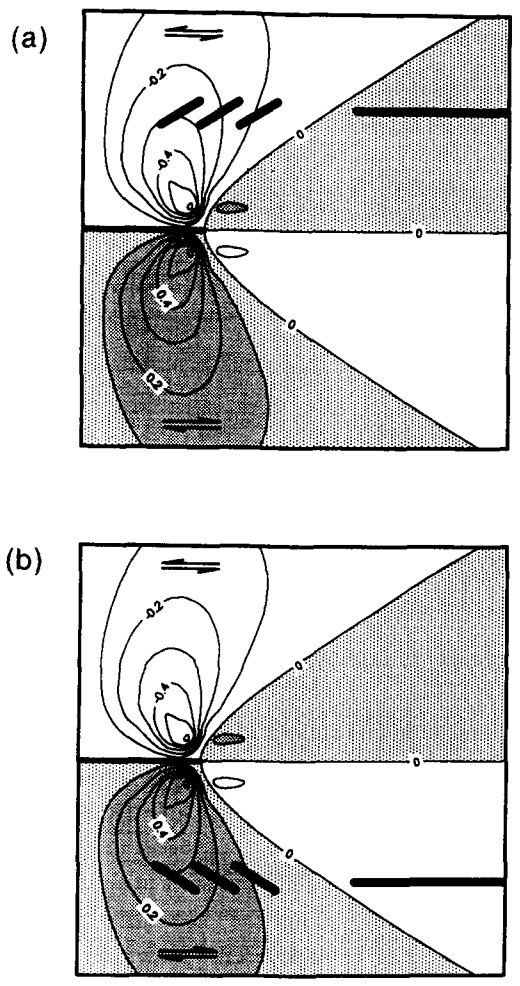

Fig. 24. Whether the echelon fractures that develop on the rising joint are twisted clockwise or counterclockwise depends on the sense of stepping of the parent joints. If the sense is right-stepping, the echelon cracks twist counter-clockwise and if the sense is left-stepping, the echelon cracks twist clockwise.

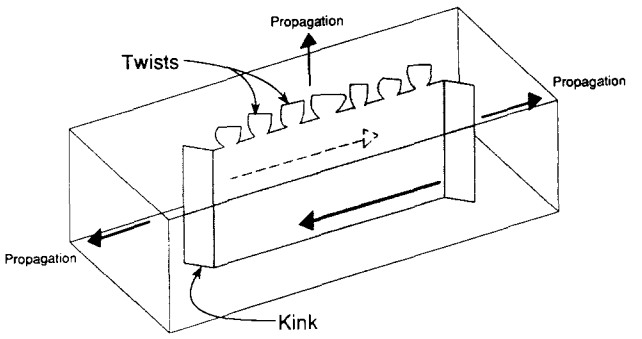

Fig. 25. An idealized parent joint propagating simultaneously upward and horizontally, with both kinks at its ends and twists at its top. The parent joint is in an environment of predominant mode I loading as well as right-lateral shear. Both the kinks and the twists are misoriented in a clockwise sense. But the twists form in mode III at the top of the propagating joint and the kinks form in mode II at the ends of the propagating joint.

Several types of minor cracks are associated with subsequent faulting of the joints. One is the kink (Fig. 4), a crack that occurs at the termination of a straight joint and whose trend is abruptly different from that of the joint. The sense of kinking indicates the sense of shear during faulting; a kink that turns clockwise with respect to the direction of the main joint is a result of right-lateral shear, and conversely counter-clockwise indicates left-lateral shear. The kink angle is related to the ratio of the shear stress responsible for the kinking to the normal stress responsible for opening the joint (equations 1b and 3b and Fig. 7a). Measurement of the kink angle at the tip and the amount of strike-slip at some point along the faulted joint provide an estimate of the amount of opening of the joint at the time it faulted (Fig. 10a), or even at the time the joint itself formed (Fig. 10b).

Although no field examples of curved kinks occur in the Garden Area, more could be deduced about the stress state if a kinked fracture was curved. Thus, if a kink curves back toward parallelism with the main joint, the normal stress parallel to the main joint was a greater compression than that normal to the main joint at the time of kinking (Figs. 11a–c and 13). If a kink diverges from the main joint, the normal stress parallel to the main joint was a greater tension than that normal to the main joint (Figs. 11e and 12).

Horsetail fractures also form near terminations of preexisting joints in response to shearing along the joint (Figs. 14a and 16). Similar short fractures can occur anywhere along the length of the joints (Fig. 16). The

primary values in recognizing these fractures is that they indicate the sense of faulting accommodated by the host fracture and the direction of maximum tension.

Even where there has been insignificant regional shearing in the Garden Area, the joints can have ornate terminations. Perhaps the most typical termination is a veer, where the end of one joint segment turns gradually toward a nearby joint segment. The veer is a result of a nearby, shear-stress-free face such as a joint surface. The most difficult feature to explain is a long overlap of parallel joint segments; that is, the lack of veer. The only plausible explanation is suggested by the research of Cottrell & Rice (1980), that high compression parallel to the joint segments will tend to prevent the joints from turning toward one another.

Perhaps the most puzzling minor fractures are the stepped joints and associated echelon cracks: puzzling because they represent opposite senses of shear. The mild misalignment of the stepped joints suggest mild left-lateral shear and the strong misalignment of echelon cracks that continue the traces of the stepped joints suggest strong right-lateral shear. Analysis of the stepped joints reflects local left-lateral shearing that acted over an area of several thousand square meters. However, analysis of the stepped echelon cracks shows that the opposite sense of shear almost certainly is a result of local interaction between the tip of one joint segment that has already broken through to the surface, and the tip of another joint segment that is growing vertically upward. Thus the echelon cracks reflect stresses that act on an area of several square meters or a few tens of square meters.

REFERENCES

Atkinson, B. K. & Meredith, P. G. 1987. Experimental fracture mechanics data for rocks and minerals. In: *Fracture Mechanics of Rock* (edited by Atkinson, B. K.). Academic Press, London, 477–525.

Aydin, A. 1978. Small faults formed as deformation bands in sandstone. *Pure & Appl. Geophys.* **116**, 913–930.

Cater, F. W. & Craig, L. C. 1970. Geology of the Salt Anticline region in southwestern Colorado. *Prof. Pap. U.S. geol. Surv.* **637**.

Cottrell, B. & Rice, J. R. 1980. Slightly curved or kinked cracks. *Int. J. Fract.* **16**, 155–169.

Cruikshank, K. M. 1991. Fracturing in Entrada Sandstone at Arches National Park, Utah, and similation of high-amplitude folding in viscous multilayers. Unpublished dissertation, Purdue University.

Cruikshank, K. M., Zhao, G. & Johnson, A. M. In press. Duplex structures connecting fault segments in Entrada Sandstone. *J. Struct. Geol.*

Dane, C. H. 1935. Geology of the Salt Valley Anticline region in southwestern Colorado. *Bull. U.S. geol. Surv.* **863**.

Davies, R. K. & Pollard, D. D. 1986. Relations between left-lateral strike-slip faults and right-lateral monoclinal kink bands in granodiorite, Mt. Abbot Quadrangle, Siera Nevada, California. *Pure & Appl. Geophys.* **124**, 177–201.

Delaney, P. T. & Pollard, D. D. 1981. Deformations of host rocks and flow of magma during growth of minette dikes and breccia-bearing intrusions near Ship Rock, New Mexico. *Prof. Pap. U.S. geol. Surv.* **1202**.

Doelling, H. H. 1985. Geologic map of Arches National Park and Vicinity, Grand County, Utah. Utah Geological and Mineral Survey Map 74 and accompanying text.

Dyer, J. R. 1979. A 3-D elastic bending-plate model for joint formation. *EOS* **60**, 944.

Dyer, J. R. 1983. Jointing in sandstones, Arches National Park, Utah. Unpublished Ph.D. dissertation, Stanford University, California.

Dyer, J. R. 1988. Using joint interactions to estimate paleostress ratios. *J. Struct. Geol.* **10**, 685–699.

Elston, D. P., Shoemaker, E. M. & Landis, E. R. 1962. Uncompahgre Front and Salt Anticline region of Paradox Basin, Colorado and Utah. *Bull. Am. Ass. Petrol. Geol.* **46**, 1857–1878.

Fleming, R. W. & Johnson, A. M. 1989. Structures associated with strike-slip faults that bound landslide elements. *Engng Geol.* **27**, 39–114.

Foering, C. 1968. The geometrical significance of natural en echelon crack arrays. *Tectonophysics* **5**, 107–123.

Lawn, B. R. & Wilshaw, T. R. 1975. *Fracture of Brittle Solids.* Cambridge University Press, London.

Martel, S. J., Pollard, D. D. & Segall, P. 1988. Development of simple strike-slip fault zones, Mount Abbot Quadrangle, Sierra Nevada, California. *Bull. geol. Soc. Am.* **100**, 1451–1465.

Nicholson, R. & Pollard, D. D. 1985. Dilation and linkage of echelon segments. *J. Struct. Geol.* **7**, 583–590.

Nicholson, R. & Ejilfor, I. B. 1987. The three-dimensional morphology of arrays of echelon and sigmoidal mineral filled fractures: data from north Cornwall. *J. geol. Soc. Lond.* **144**, 79–83.

Olson, J. & Pollard, D. D. 1988. Inferring stress states from detailed joint geometry. In: *Key Questions in Rock Mechanics* (edited by Cundall, P. A., Sterling, R. L. & Starfield, A. M.). *Proc. 29th U.S. Symp. on Rock Mechanics.* A. A. Balkoma, Rotterdam, 159–167.

Olson, J. & Pollard, D. D. 1989. Inferring paleostresses from natural fracture patterns: A new method. *Geology* **17**, 345–348.

Ohlen, H. R. & McIntyre, L. B. 1965. Stratigraphy and tectonic features of Paradox Basin, Four Corners area. *Bull. Am. Ass. Petrol. Geol.* **49**, 2020–2040.

Pollard, D. D. 1976. On the stability of open hydraulic fractures in the earth's crust. *Geophys. Res. Lett.* **3**, 513–1204.

Pollard, D. D. & Aydin, A. 1984. Propagation and linkage of Oceanic Ridge segments. *J. geophys. Res.* **89**, 10,017–10,028.

Pollard, D. D. & Aydin, A. 1988. Progress in understanding jointing over the past century. *Bull. geol. Soc. Am.* **100**, 1181–1204.

Pollard, D. D. & Holzhausen, G. 1979. On the mechanical interaction between a fluid-filled fracture and the earths surface. *Tectonophysics* **53**, 27–57.

Pollard, D. D. & Segall, P. 1987. Theoretical displacements and stresses near fractures in rock: with applications to faults, joints, veins, dikes, and solution surfaces. In: *Fracture Mechanics of Rock* (edited by Atkinson, B. K.). Academic Press, London, 277–349.

Pollard, D. D., Segall, P. & Delany, P. T. 1982. Formation and interpretation of dilatant echelon cracks. *Bull. geol. Soc. Am.* **93**, 1291–1303.

Rubin, A. M. & Pollard, D. D. 1988. Origins of blade-like dikes in volcanic rift zones. *Prof. Pap. U.S. geol. Surv.* **1350**, 1449–1470.

Segall, P. 1984. Formation and growth of extensional fracture sets. *Bull. geol. Soc. Am.* **95**, 454–462.

Segall, P. & Pollard, D. D. 1983a. Joint formation in granitic rocks of the Sierra Nevada. *Bull. geol. Soc. Am.* **94**, 563–575.

Segall, P. & Pollard, D. D. 1983b. Nucleation and growth of strike-slip faults in granite. *J. geophys. Res.* **88**, 555–568.

Sumi, Y., Nemat-Nasser, S. & Keer, L. M. 1985. On crack path stability in a finite body. *Eng. Fract. Mech.* **22**, 759–771.

Tada, H., Paris, P. C. & Irwin, G. R. 1985. *The Stress Analysis of Cracks Handbook* (2nd edn). Paris Productions, Inc., St. Louis, Missouri.

Zhao, G. & Johnson, A. M. In review. Sequence of deformations recorded in jointed-faults and faulted-joints, Arches National Park, Utah. *J. Struct. Geol.*